DYNAMIC, IN-SITU PRESSURE MEASUREMENTS DURING CMP

A Thesis
Presented to
The Academic Faculty

By

Andrés Osorno

In Partial Fulfillment
Of the Requirements for the Degree
Master of Science in Mechanical Engineering

Georgia Institute of Technology
December 2005

DYNAMIC, IN-SITU PRESSURE MEASUREMENTS DURING CMP

Dr. Steven Danyluk
School of Mechanical Engineering
Georgia Institute of Technology

Dr. Shereyes Melkote
School of Mechanical Engineering
Georgia Institute of Technology

Dr. Steven Liang
School of Mechanical Engineering
Georgia Institute of Technology

Date Approved: September 23, 2005

ACKNOWLEDGEMENTS

I would like to thank all the people that made this thesis possible. I would especially like to acknowledge my graduate research advisor, Dr. Steven Danyluk for his support and advice. I would like to especially highlight his support for new ideas, as well as the maintenance of a very well equipped laboratory where many things are possible.

I would like to thank all the members of our research group that at some point or another have helped me with some idea or concept to try. Thanks to my brother Daniel, Fang, Frank, Gregorio, Shijiang, and Yury for their help. I would especially like to thank the CMP group, Gary and Inho, for teaching me about the CMP process, idealizing some of the concepts included in this thesis, and giving my research some direction. I would also like to thank Siarhei for his design and fabrication of the wireless circuitry and the programming of the wireless board. I would also like to express my gratitude to Ms. Rogers and Ms. Teasley for their support in the administrative side. Also many thanks to Dr. Leonard Borucki for the continuous feedback on related CMP models and results, as well as suggestions for improvement.

Finally, I would like to recognize my parents Ivan Dario Osorno and Dolly Gomez and my sister Isabel Cristina for their many contributions. They supported me economically throughout my undergraduate studies at the Georgia Institute of Technology, as well as morally during my graduate studies. I know they are proud of my accomplishments, and this kept me on aiming for my goals. Thanks for all your support.

TABLE OF CONTENTS

LIST OF TABLES

LIST OF FIGURES

SUMMARY

A rotational setup for measuring interfacial fluid pressure and temperature was successfully constructed. Interfacial fluid measurements were performed with various slurry types, slurry flow rates, and pad topographies. It was experimentally determined that the pad topography has the biggest effect in pressure and temperature distributions. This was also confirmed by tilt experiments ran in a rotational environment. For all cases, the edge high conditioned pad displayed the most changes during the experiments.

For an edge high conditioned pad, the fluid pressure was found to be mostly subambient reaching levels of up to 42 kPa at the center of the fixture, and dissipating towards the edges. The pressure maps appear to be almost center symmetric. The pressure was found to be positive during the first second of contact, and rapidly turned subambient. The subambient pressures stabilize after about 5 seconds, and the suction force created was found to significantly slow the rotating platen. Suction forces were confirmed by disk displacements observed during the tilt experiments. The fixture's center was sucked down into the pad up to 20 µm, and tends to tilt towards the leading edge.

Interfacial temperatures were also found to vary with pad geometry. The edge-high conditioned pad exhibited changes of up to 4 °C, concentrated at the center. The relative position and shape of these temperature rises matches the results observed in the pressure experiments. Temperature takes a longer time to reach equilibrium, up to 30 seconds in most measurements.

Other pads used in the experiments (unconditioned plain pads and k-groove pads) exhibited very little pressure or temperature development. In the case of the k-groove pad this can be explained by the release of pressure under the grooves. The unconditioned pad exhibits positive pressures only, possibly due to hydrodynamic lubrication.

CHAPTER 1
INTRODUCTION

For the successful manufacture of integrated circuits (IC), high levels of planarity are required. Chemical mechanical polishing (CMP) is a process used by IC manufacturers to achieve both local and global planarization of the wafer surface. CMP has been recognized as the most effective method to achieve global planarization in very large scale integrated circuits (VLSI). One of the uses of CMP is the removal of undesired topography in interlevel dielectric layers (ILD) and tungsten plug processing. Studies have demonstrated that polishing of the tungsten plug structure using CMP is more controllable and results in a higher yield than with the typical etch back process [1]. CMP is also used during the damascene process, where metal is deposited on ILD and later the higher blanket deposit is removed. Multilevel interconnects require the planarization of the surfaces for subsequent device processing. Lack of planarity may lead to problems during photolithography and etching, especially as the size of features decreases [2].

The CMP process closely resembles a lapping process, in which the surface of a silicon wafer is pressed against a resilient surface, and slurry consisting of oxidizing chemicals and fine abrasives is entrained between them [3]. The slurry is very important for the process since the polishing surface (pad) is usually much softer than the material being removed. The combination of the hard abrasive particles in the slurry and the oxidizing properties of the chemicals ease the removal of material during CMP. The interaction between the wafer surface, the pad, and the abrasives in

the slurry provide mechanical removal, while the oxidizing slurry chemistry facilitates the removal process.

Despite the wide range of use of the CMP process in IC fabrication, many aspects of the process are not well comprehended. This hinders the ability to produce composite models or simulations to estimate response parameters such as material removal rate, selectivity, planarity, dishing, erosion, etc. During the CMP process, generally both surfaces (the polishing pad and surface to be polished) are in relative motion, while the slurry is continuously being delivered in anticipation of the outermost point of contact. This provides for a very complicated process, in which the material removal rate at the wafer depends on the various components, each with its own set of variable parameters: the polishing machine, the slurry, the polishing surface, the pad, and the interactions between them. Little is known about what is occurring underneath a wafer during CMP.

Figure 1.1 displays the configuration of the pressure measurement experimental apparatus, which resembles a typical CMP process. The typical CMP setup consists of a CMP machine which provides lapping motions to a platen, containing the polishing pad, and a rotating head which carries the wafer. The wafer is held in place through a wafer carrier, which prevents it from sliding out. Both surfaces are in rotation when they come into contact with each other, and a uniform load is applied onto the carrier to achieve the desired contact between the surfaces. Generally, both surfaces rotate in the same direction. In some cases a sweeping motion is applied to the head to vary the contact speed of the wafer against the large polishing pad. The slurry is delivered by the system ahead of the wafer-pad interface.

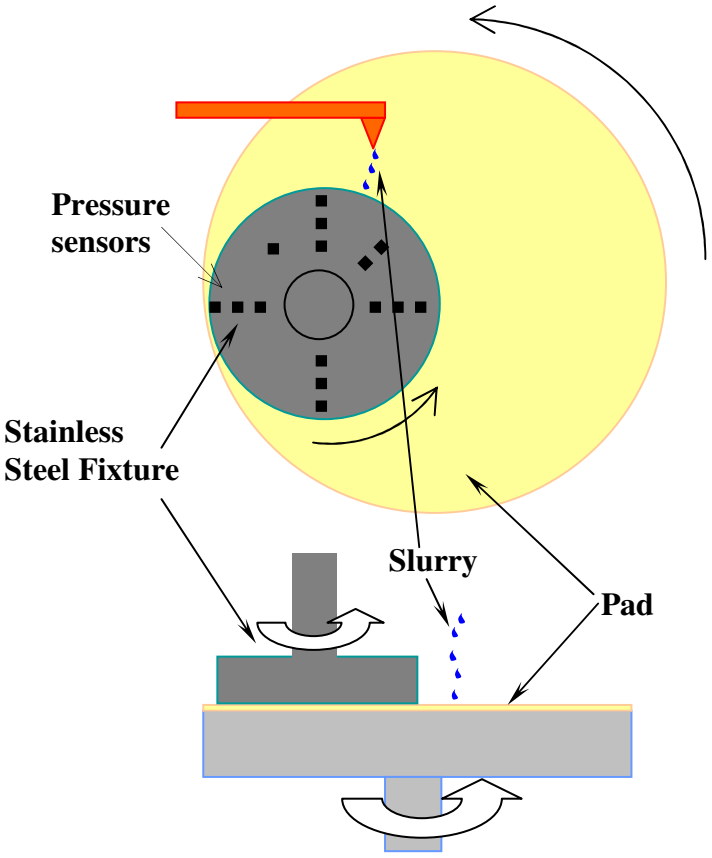

Figure 1. Typical CMP Setup

During a CMP process, the stainless steel fixture depicted in Figure 1 would be replaced by a wafer carrier. A wafer carrying fixture is able to hold wafers of a predetermined size by using an adhesive backing, vacuum, a porous membrane, or other such materials. Figure 2 is a representation of an actual wafer carrier fixture used at the Electronic Material Lab (EML) at Georgia Tech during a series of copper CMP experiments.

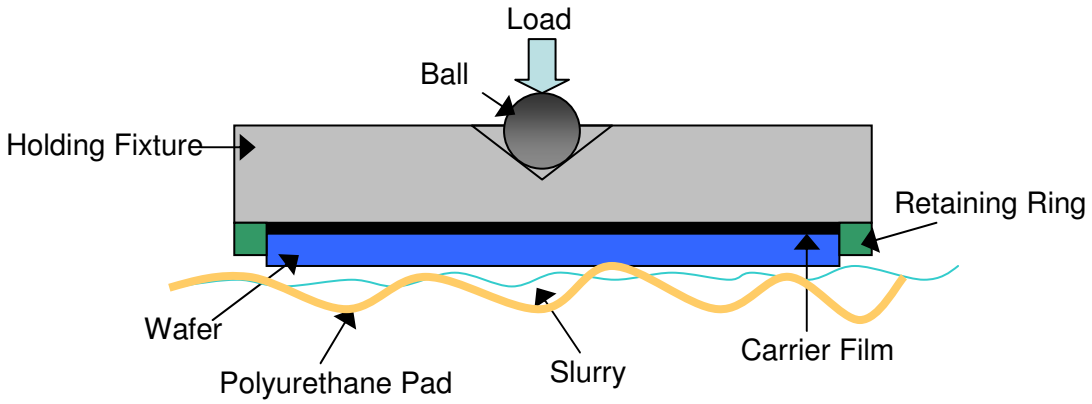

Figure 2. Wafer Carrier Setup

Among the difficulties that CMP faces are the polishing of new materials, tight planarization requirements (due to feature sizes), and application to large diameter wafers (which have increased to up to 300mm in diameter). Both chemical and mechanical mechanisms have been identified as contributing factors of the removal phenomenon; however, the relative contribution of each is still poorly understood. CMP material removal models usually employ a variation of Preston's formula, which was developed for glass polishing, to relate material removal rate to process conditions. Equation 1 displays Preston's equation, which describes the basis of polishing rate during CMP.

$$MRR = k \times P \times V \qquad \text{Equation 1}$$

Preston's equation implies a linear variation of material removal rate due to contact stress (P) and polishing velocity (V), with Preston's coefficient (k) used to describe other process parameters. This relationship is simplistic, due to the complicated nature of the CMP process, and usually incorporates several variables such as process temperature, chemical action, slurry effects, and others into the variable *k*. Such analyses assume that the pad/sample interface geometry remains

invariant with time, which is not always the case during CMP [4]. Variations of Preston's equation usually change exponents for P and V due to their relative contributions to the polishing process, as well as study the effects of other process parameters, which are imbedded into *k*. Fluid behavior beneath the wafer is one of the most important factors that dictate the polishing mechanism (as it can affect the distribution of pressure (P) on the wafer side), as well as dictate the lubrication regime [5]. It is important to develop a device that obtains direct pressure measurements while the wafer is rotating, with a minimum effect on other process parameters [6].

Previous CMP work at the Georgia Institute of Technology has focused on measuring interfacial fluid pressure and studying the contributions of polishing parameters in the development of these pressures. Levert and Danyluk first discovered the existence of subambient pressures during CMP by measuring the vertical displacement of the wafer and the frictional drag under typical polishing conditions. They found that the wafers were drawn closer to the pad, indicating the existence of suction pressures at the interface. Later experiments focused on changing process parameters such as speed, load, slurry particle size, fluid film thickness, and pad surface roughness to measure their influence in the magnitude and location of the subambient pressures. All of the previous experiments were performed in an environment where the pad rotated while the wafer fixture did not. This was due to the wire connections used for data acquisition.

This thesis investigates fluid pressures that occur in the wafer-pad interface, as well as the development of interfacial temperature during a polishing process where

the pad and the wafer fixture both rotate. The fluid pressure at the interface is found to be non-uniform throughout the area of the wafer, affecting the contact area and pressure at the interface, thus changing the material removal rate at the polishing surface. Local temperature variations influence the material removal rate at the interface by affecting material properties of the pad and the polishing surfaces, as well as the reaction rate at which the polishing process occurs.

The layout of this thesis is as follows: Chapter 2 contains a literature review which encompasses the main topics and parameters studied in this thesis, including the CMP pad characteristics, pad conditioning, CMP process temperature, interfacial fluid pressure, and a review of previous work done in this area at the Georgia Institute of Technology. Chapter 3 has a description of the system design and architecture, including mechanical devices, electronic devices, and software implemented to manage the various devices built for the purpose of this work. In Chapter 4, a description of device calibrations, system verification, and noise reduction efforts follows. Chapter 5 contains information regarding the experimental setup, the experimental variable settings, and experimental procedure followed during all data acquisition efforts. Chapter 6 has information regarding the main differences between static and dynamic experiments, as well as pressure, temperature, and tilt measurement results. Chapter 7 contains closing remarks and conclusions.

CHAPTER 2
LITERATURE REVIEW

CMP should be viewed as a system, since many variables are present at the same time and some may interact with each other affecting process performance. Among the output parameters being monitored during CMP are material removal rate, within wafer non-uniformity of material removal, wafer-to-wafer non-uniformity, degree of planarization, and surface defects. Within wafer non-uniformity (WIWNU) is commonly measured as the standard deviation of the thickness removal measurements expressed as a percent of the average thickness removed. Wafer-to-wafer non-uniformity (WTWNU) is the standard deviation of removal rate for a number of wafers in a batch. Degree of planarization is the step height reduction expressed as a percent of pre-process step height [7]. All of these performance parameters are dependent upon the various process parameters that exist in CMP, some of which are investigated in throughout this thesis.

The process parameters investigated in this thesis are: the CMP pad and conditioning, surface temperature, fluid pressure of the slurry entrained between the pad and the wafer, and slurry flow rate. This section presents an overview of the existing literature and research in these areas, as well previous work at the Georgia Institute of Technology with regards to CMP technology.

The CMP Pad

Planarization performance in CMP is significantly influenced by the polishing pad characteristics. The CMP pad transmits mechanical energy to the substrate as well as transports the slurry for polishing. The pad is manufactured by the mixing of a urethane polymer, a pore forming agent, and a curing agent. The mixture is poured into a mold and allowed to cure before the cake is taken out and sliced into individual pads [3]. Different types of pads are used during CMP including porous polyurethane, non-woven pads, and artificial suede among others. The most widely used type of pads is a combination of the IC1000 and SUBA IV pads in a stacked form [8] manufactured by Rodel Inc. Stacked pads are usually built in the following manner: A polyurethane foam layer (IC1000), a polyurethane coated felt (SUBA IV) laminated via a pressure sensitive adhesive (PSA 5), and another pressure sensitive adhesive (PSA 2) used to adhere the stacked pad to the polishing platen. PSA 2 & 5 are both polyester films with adhesives on both sides. The overall elastic properties of the stacked pad are a weighted combination of the properties of its components, proportional to their relative fractional amount [9]. IC1000 pads are made of a micro porous polyurethane (viscoelastic) material and provide a rigid surface which is very desirable for ILD planarization. SUBA IV pads are made of polyurethane impregnated polyester felts and have a rougher surface than IC1000 pads, which allows them to hold the slurry better [10]. The pad surface is porous, having between 30-35% void content per unit volume, 1.35mm in thickness, and in a cross sectional view appears to have around 50% of its area covered by voids [11][12]. The pads' top layer is also permeable and when soaked for extended periods of time (24 hours or

more), its elastic modulus changes significantly. The bulk of the pad is not affected by the immersion in water, which suggests lower permeability. Water is believed to disrupt the hydrogen bonding of the polyurethane chains, affecting the elastic modulus [13][14]. Results of pad soaking experiments at the Georgia Institute of Technology show that there is an increase in the magnitude of the sub-ambient pressure with increasing pad soaking time. There is a sharp increase in pad weight (due to absorbed water) during the first 50 hours of soaking. The pad weight then reached a steady state after 100 hours. No change in size of the pad was measured. Weight increases by about 4 to 4.5%. Weight increase was found to be better correlated to surface area than volume, indicating that water absorption is limited by the outer layer of the pad. This was confirmed by using ink in the water, and observing the water penetration into the pad through the use of microscopes [3]. Obeng *et al.*[15] also determined that polyurethane pads degrade principally from chemical attack during its use. After drying, the pads' original elastic modulus is reestablished. The pad's elastic properties are important to CMP, as they contribute to the direct wafer-pad abrasion and indirectly to the pad-slurry-particle wafer abrasion. The reduction in elastic modulus makes the pad softer, and reduces its polishing ability [13][14][15]. Pad surface characteristics are important because they affect the real area of contact, friction, wear, and lubrication at the interface. Reduction in elastic modulus was found to be approximately 30% in soaking periods of over 24 hours [14]. As the pad modulus decreases, there is more asperity deformation, more contact area, and less load on individual asperities which causes a reduction in the polish rate. This has been proven experimentally and confirmed by the Greenwood-

Williamson micro contact model [13]. The dynamic shear modulus of the pad also decreases with soaking time, up to two-thirds within five hours of soaking. However, the oxide removal rate of the pads appears unchanged by the penetration of water [10]. Deterioration of the pad resulting from the combination of blockage of slurry transport channels and pad deformation also causes a drastic reduction in polishing rate [16].

Pads are made with different surface patterns. Examples of patterns are: plain pads (no pattern), k-groove pads (with center symmetric circular grooves), perforated (with holes punched through them at specific locations), among others. Slurry transport dynamics of the different pads is an important factor that influences the material removal rates [8]. In the case of a k-groove pad, grooves allow the slurry to be efficiently "squeezed out" from underneath the wafer carrier, thus reducing lubrication and enhancing wafer-pad contact [17]. Other slurry transport studies have been conducted using laser induced fluorescence measured by digital cameras. These studies measured mixing and temperature, as well as film thickness [5]. The experiments consisted of a clear glass disk (simulating a silicon wafer) which was subject to various polishing conditions. Dyes were added to the slurry for the purpose of being captured by the cameras. A digital analysis of the images captured was then used to study the slurry transport mechanisms in the wafer-pad interface. Pads have also been studied during dynamic mechanical analysis to investigate the mechanical properties of the pad, more importantly its ability to store and dissipate mechanical energy upon deformation in a dynamic situation [9].

There is ample research in the area of polishing pads, not only for their importance as a consumable in a widely used process as CMP, but also for the effects it incurs to the final polishing quality, depending on its characteristics. Various advanced metrology techniques such as x-ray photoelectron spectrometry (XPS), scanning white light interferometry, atomic force microscopy (AFM), and scanning electron microscopy (SEM), that in conjunction with other tools, have been all been used to analyze pad wear and morphology effects of CMP on the pad [18].

CMP Pad Conditioning

Pad conditioning is a crucial step in CMP, as the oxide removal rate decreases with time when the pad is not being conditioned until reaching a low steady state value [10] [19].There is a clear relationship between the decrease in polish removal rate and the reduction of asperity height on the pad due to the CMP polish removal rate sensitivity to the structure of the CMP pad [19]. Pad surface conditioning is a process commonly used before and during CMP. A diamond disk or hard metal-plate rubs against the surface removing damaged surface layers, disposing of accumulated abrasive and polished oxide or metal particles, and increasing the pad surface roughness. The conditioner is a circular disk with diamond tips that protrude a certain amount. The abrasive wheel spins at the end of the conditioner arm, while it is being swept across the length of the moving pad. Conditioning density (CD) is defined by Equation 2, where V_{arm} is the velocity of the arm in the radial direction, while R is the radial position on the pad.

$$CD = \frac{1}{V_{arm} \times R_{pad}}$$ Equation 2

Higher conditioning density equates to higher geometric pad wear by the abrasives [20]. The conditioning process can also provide for a large source of wafer contamination in the form of abraded pad material which needs to be controlled to maintain the integrity of the devices being polished [21].

The surface of a new (unconditioned) pad is smooth and wets poorly because of the closed-cell polyurethane. This reduces its ability to effectively transport the slurry to the wafer-pad interface. Conditioning opens up closed cells, improves slurry transport, and provides a consistent polishing surface [22][23]. The "break in" process of pads (pads are conditioned for long periods of time prior to first being used) minimally affects the pad's thickness. Polishing was found to decrease the pad's thickness significantly [21]. During pad conditioning, all variables (type and abrasiveness on the disk, disk size, conditioning down force, speed of conditioning disk, time, and location) are all closely monitored to produce desired results. A less than optimum conditioning process results in a relatively rapid degradation of the removal rate. A very aggressive conditioning makes it unstable over the long run while decreasing pad life. Both cases result in high WTWNU [7]. Lawing at Rodel (the major IC pad manufacturer) investigated the ability to manipulate the pad's conditioned surface by changing parameters such as the diamond crystal size, diamond crystal morphology, and crystal surface density [24]. In his work, Lawing was able to vary these parameters to achieve the desired pad profile for various CMP applications. He found that the effect of the pad-conditioner contact was that of restoring and maintaining a random distribution of surface asperities through the

renewal of damaged material. Lawing also found that the effect of the pad-wafer contact on the pad is to deform the pad surface asperities. Coppeta *et al.*[5] found that diamond conditioning increases the thickness of the slurry layer between the pad and the wafer, but has a negligible effect on slurry mixing under the same interface.

Degradation of ILD removal rate and short pad life are serious concerns with CMP technology. Glazing of the pad surface and inadequate pad conditioning are primary causes of the reduction in material removal rate. Glazing of the pad decreases its slurry holding capacity which in turn reduces material removal rate due to reduced chemical and mechanical attack to the polishing surface [10]. Typically, material removal rate drops progressively as more wafers are polished without any kind of pad conditioning. This reduction in rates makes it difficult to maintain a stable manufacturing process. Suitable pad conditioning is the key to stable removal rates [16]. Studies have revealed that pad conditioning maintains a uniform material removal rate while decreasing planarization efficiency [10]. Two ways of conditioning the pad are commonly used: In-situ conditioning refers to conditioning the pad while the polishing is in process, usually in advance of the pad contacting the polishing surface. Ex-situ conditioning usually occurs in between polishing wafer batches or when the pad surface is determined to be significantly worn. In-situ conditioning has shown an increase in material removal rate when compared to ex-situ conditioning, especially if glazing occurs [25]. In some cases, material removal increases with in-situ conditioning by 15-20%, while at the same time increasing within wafer uniformity by 23-45% [16]. Iqbal *et al.*[22] found that non-uniformities deteriorate with unconditioned pads.

In conditioning, only the top layer of the pad is renewed by the conditioner. This is sufficient since the alkaline media from the dielectric polishing slurry (which degrades the polyurethane material through hydrolytic attack) only comes into direct contact with top surface of the pad [9]. Pad deformation is directly proportional to the applied stress and not so much with its speed. The contribution to pad deformation by compression is small when compared to the wear caused by the conditioning process [16]. Due to conditioning, the pad gradually takes a certain profile. This pad profile can help or hurt WIWNU, depending on the profile [7]. One of the purposes of this thesis is to investigate how a certain pad profile affects the fluid pressure distribution along the wafer surface and its consequences on planarization.

Process Temperature

As with any material removal process, CMP generates heat. This heat is generated by the mechanical shear of the pad and the abrasive particles against the substrate, the exothermic chemical reaction of the slurry during chemical etching, and by dissolution. Pad temperature is used as an end-point detection metrology based on the energy released during the CMP process. Tracing the pad temperature can effectively monitor the removal rate during metal CMP [26]. Various efforts by investigators include measuring, quantifying, explaining, and modeling heat generation during CMP. CMP models usually rely heavily on parameters such as pressure, velocity, slurry abrasive particle composition, and pad properties to characterize material removal rates. Temperature, which potentially influences both mechanical and chemical removal processes, is often neglected [27]. The importance

of process temperature is such that for example, the formation of copper oxide has an activation energy of only 0.6 eV. A temperature increase of 10 ^{o}C is sufficient to double the removal rate, and fluctuations of only 1 ^{o}C would be noticeable throughout the area of a polished wafer [28]. The temperature distribution under the wafer-pad interface is a function of many of the CMP process parameters including load, speed, surface topography, material properties of the pad and the substrate, slurry chemistry, and the environment, among others [6]. Temperature information is critical for establishing pad life and for the design of pads with stable dynamic mechanical properties which can provide a more uniform material removal rate across the wafer [29].

Experiments in CMP's process temperature have mainly focused on the pad temperature or slurry temperature under typical polishing conditions. Dynamic Mechanical Analysis (DMA) is the main technique used for the study of process temperature during CMP. DMA has provided a clear indication of pad property changes with temperature and usage [9]. It was observed that the shear modulus of the polishing pad decreases with an increasing pad temperature. In IC1000 pads, temperature changes from 40-80 ^{o}C and 30-90 ^{o}C decrease the pad's shear modulus by a factor of 2 and 3 respectively. The increase in temperature also caused an increase in oxide removal rate and planarization efficiency (the step-height reduction per unit oxide removed on the "up feature") [10]. At Intel Corporation [30], it was found empirically that the slurry temperature could raise approximately 20-30 ^{o}C during CMP. Pad characterization using DMA showed that the pad's storage modulus, G', can decrease up to 31% under normal CMP conditions. Part of the decrease in the

storage modulus and some pad deformation changes are attributed to temperature changes during the polishing process [31]. It was also determined that the coefficient of thermal expansion (CTE) does not change during the typical temperature operating region (25-50 ^{o}C). Sorooshian *et al.*[29] found that in polyurethane pads the flexural storage modulus (a parameter used to describe the bulk softening of the pad) decreases up to 42% with increasing polishing temperatures. The softening of the pad increases the shear force experienced by the polishing surface because the softer pad will become further compressed by the applied normal load. Also, pad asperities in the wafer-pad interface tend to collapse due to the softness of the pad. Experimental results show that increasing platen temperature increases the coefficient of friction (COF) for ILD and copper processes due to the previously discussed softening of the pad [27][29]. The average coefficient of friction can be calculated using Equation 3, and is linearly related to material removal rate.

$$COF = \frac{F_{shear}}{F_{normal}} \qquad \text{Equation 3}$$

Several experimental studies have been conducted to quantify heat generation during CMP. A study aimed at quantifying the contribution of temperature in thermally dependent and thermally independent aspects of CMP was performed. This study presented a modified version of Preston's equation that included temperature effects such as activation energies. The experiments were conducted using an infrared camera to record the pad surface temperature using 5 points around the leading edge, and 5 points around the trailing edge of the wafer. These points measured pre and post pad-wafer contact. Results showed that the total fluctuation was not more than 4^{o}C [27][29]. Thermal effects were shown to be small in magnitude and transient in

nature (temperature rises during the first 30 seconds of a 75 second polishing process and remains constant thereafter) [6][29]. Frictional force measurements show that the COF drastically drops during the first period of polishing time [6]. Results also show that despite variations in pressure and velocities during experimentation, the effects of temperature on material removal impacted all conditions in a similar and relative manner. The ILD polishing process shows a Preston constant dependency on temperature of around 8%. The average thermally dependent contribution on Preston's constant for copper CMP was 62% [27]. The dramatic rise in temperature dependency can be attributed to chemical factors being more dominant during copper polishing. Karaki and Watanabe [32] found that the activation energy of the work surface decreases as a result of a rise in work surface energy, and that this results in an increase of material removal. In CMP, the removal rate is particularly influenced by the magnitude of the chemical action which is activated by a rise in temperature and crystal surface strain (caused by mechanical action of abrasives and polishing pad contact). The speed integral (calculation of the relative velocity at every point on the wafer) and infrared data from the pad agree. The speed at the edges is faster and they polish faster. Temperature also decreases with wafer count, as well as polish rate (due to deterioration of the pad and a lower COF) [33].

In-situ endpoint detection mechanisms for CMP of tungsten and barrier Ti / TiN have also been experimentally created. This device was based on the principal that the pad surface temperature increases as metals are being polished, but significantly drops when the oxide layer is reached. The temperature increase is due to the creation of a tungsten oxide passivation layer (exothermic reaction) and the

later abrasive removal of it which generates frictional heat [34]. Unfortunately, all of the previous attempts to measure CMP process temperature have used pad or slurry temperature before and after the contact with the polishing surface. Cornely *et al.*[35] studied how wafer-pad relative velocities, wafer pressure, and wafer curvature affected the evolution of thermal characteristics. Results concluded that for a convex wafer, film thickness decreases as pressure is increased (higher pressures tend to compress pad asperities in contact with the outward curve of the wafer). Film thickness does not change for a concave wafer (high asperity compression around the edge makes it unable to move any closer to the pad as the pressure is increased). Film thickness increases with pad speed in convex wafer (partially hydroplaning) and decreases for concave wafers because of suction. Increasing pressure increases wafer temperature in both cases. Real time temperature measurements in the pad-wafer region can allow for the decoupling of chemical and mechanical contributions to friction force and material removal rate during CMP. The lack of knowledge regarding the local heat evolution and distribution in the wafer interface is one of the problems addressed in this thesis.

Slurry chemistry and composition can also be affected by the changes in temperature during CMP. It was experimentally demonstrated that the pH value of the slurry decreases with increasing temperature. The change in pH with temperature is caused by a shift in the equilibrium state between $[H_3O]^+$ ions and $[OH]^-$ ions since the equilibrium is affected by absolute temperature. A high temperature polishing process has also the potential to cause scratching due to an increase in kinetic energy of the dispersed abrasive particles, which increases their collision rate and size [6].

Interfacial Fluid Pressure

Interfacial fluid pressure in CMP is one of the key factors that affect polishing rates and uniformity. Most of the research in this area has focused on computational mechanics and fluid dynamics, final element analysis (FEA), and the use of various forms of the Navier-Stokes and Reynold's equations. Empirical research has been conducted to measure fluid pressure, mostly in a static environment, while simulating CMP polishing conditions. Extensive work has been performed at The Georgia Institute of Technology to characterize interfacial fluid pressures during CMP, as well as to develop computational models that predict these pressures under various conditions.

Various methods of maintaining a uniform pressure distribution at the wafer level have been tested experimentally. Many applications of CMP use a uniform backpressure during polish. Three parameters of backpressure are usually varied: Magnitude, direction (positive or negative pressure), and position (where the backpressure is applied on the wafer). In most cases, wafer backpressure is applied through holes in the wafer backing plate on the wafer carrier. Wafer backpressure adjusts the bow of the wafer, adjusting the fluid and contact pressure exerted onto the wafer at the polishing interface. For a new polishing pad and a wafer backpressure of zero, oxide removal tends to be higher in the wafer center [36]. Melvin *et al.*[37] developed an axiomatic fixture to insure an even applied pressure on the back of the wafer. An intricate pocket of water behind the wafer and carrier film was used. The water pressure was controlled through the entire wafer area to insure uniformity. This axiomatic design was developed for the purpose of reducing within wafer non-

uniformities. In other studies, final element methods (FEM) were used to determine the contribution of different wafer and holder geometries with respect to pressure distributions. It was determined through FEM that chamfering the wafer edge resulted in more uniform distributions. It was also deemed as beneficial to the uniformity of the pressure on the wafer to polish in the presence of a retaining ring [38].

During CMP, wafer rotation is used to average out gross material removal rates and improve within-wafer thickness uniformity. Fluid transport between the wafer and the pad surfaces is strongly affected by pad macrostructure and relative motion of the two surfaces. A phenomena known as the “edge defect” occurs when the reduction of fluid velocity as the slurry stream passes between the wafer and pad causing suction pressure which pulls down the leading edge of the carrier. This effect is consistent with enhanced contact between the wafer and pad at the leading edge which results in increased material removal rate. The leading edge effect (high material removal rates at the leading edge of the wafer while very low at the trailing edge) is an important phenomena encountered in CMP in the absence of rotational averaging. Rotation converts leading and trailing edge gradient in material removal rate into radial non-uniformity. Rotational polishing results show a more stable removal process, yielding center fast profiles which are typical of actual polishing processes and are often observed in industry. A lower gimbal location would help mitigate the problem, providing a smaller angular deflection of the wafer carrier [17].

Pressure on the silicon wafer is dependent upon many different aspects during the polishing process. One of these variables that determine interfacial pressure is the patterns printed on the wafer face. For example, the effective pressure experienced by

STI patterned wafers according to their pattern density is not proportional. As the density of the patterns increases, the pressure decreases [39]. Wafer bowing and warping are also factors that influence pressure distribution along the surface of the polishing surface. Concave or convex bowing of the wafers would increase the difficulty of flattening the wafer when pressed against the polishing pad. This defect may eventually lead to a non-uniform pressure distribution, since these defects on the bulk silicon transfer though the thin films that may be deposited onto the wafer and eventually lead to selective high removal rates of the deposited material. Zhang *et al.*[40] investigated the effects of bowing in material removal rate and concluded that removal rate appears to be a function of pre-polish wafer bow, decreasing as the shape changes from concave to convex. For concave wafers, the polishing results were edge high, while for convex wafers, the polishing results were center high. Highly curved areas tend to lead to high removal.

In-situ fluid pressure experiments have been previously performed [41]. In these sets of experiments, a strong vacuum was generally observed when using flat wafers (3-5 µm center to edge) and therefore follow-up experiments were conducted using a wafer that was polished to a convex shape of 50 µm center to edge. Signal was acquired by a pressure transducer and transmitted by pressing the rotating sleeve and its contacts against the signal contacts. The device measures the pressure of the wafer-pad interfacial film during CMP with several sensors located throughout the wafer area, but only being able to measure one sensor per trial run. The experimenters were able to determine that the relative motion between the pad and the wafer creates a fluid wedge approximately 10-60 µm thick as slurry is drawn in. Stationary trials

resulted in asymmetrical pressure distribution, with two pressure peaks and two pressure troughs under the wafer. The two peaks were located where the pad speed was highest and lowest. The two troughs consisted of sub-ambient pressures at the leading and trailing edges of the wafer. Dynamic trials displayed less variability, with pressure increasing monotonically from edge to center. There was not much change within one sensor when compared to its angular position [41]. Changing the flatness of the silicon wafer that is used for experimentation can influence the results obtained (as previously explained, wafer bowing affects pressure distributions along the wafer), yet it is important to point out that Bullen *et al.*[41] were able to find radically different results between static and dynamic data.

Various other experiments regarding interfacial fluid pressure have been conducted at the Electronic Material Laboratory (EML) at the Georgia Institute of Technology. Both empirical data and analytical models have been developed, encompassing various CMP variables that affect such distributions at the wafer-pad interface. A summary of these results is presented in the following section

Previous Work

CMP research at the EML at the Georgia Institute of Technology has been an ongoing process at investigating how certain process parameters affect material removal rate. This work can be divided into two main topics: Investigation of the effects of particle size distribution in commercially available slurries for CMP and the characterization of fluid pressures and lubrication regime at the wafer-pad interface. The majority of this work has been published and serves as an important resource for

this thesis. First, studies of the effects of abrasive particles in the removal rate will be presented, followed by a description of previous interfacial fluid characterization efforts and results.

Material removal rate during CMP is sensitive to the abrasive particle's size. There exists an optimum abrasive size with respect to material removal rate and surface finish, given a set of experimental conditions. It was found experimentally that a certain particle size exhibited higher material removal under the predetermined polishing conditions, and that polishing rate in all instances varied linearly with the interaction effect of pressure and peripheral speed at the wafer-pad interface, complying with Preston's equation (Equation 1). This indicates that there was no "suction" pressure between the polished wafers and the pads used (grooved) [42]. In other experiments, an evanescent-wave visualization technique was developed to observe the dynamics of fluorescent colloidal silica particles in the slurry. This setup also made it possible to measure the velocity and concentration of the interfacial particles during the polishing process. These experiments served as a great insight into how the abrasives in the slurry behave at the pad-wafer interface, which is important for the realization of any abrasive model for material removal rate in CMP [43].

The bulk of CMP research performed at the EML is related to tribological aspects of this polishing process. Part of this effort has been focused around parameters such as fluid film thickness, pad surface roughness, pad material properties, interfacial fluid pressure, wafer bowing, and wafer tilting. All of these efforts intend to understand the interface mechanisms that give rise to non-

uniformities in CMP, in an attempt to improve overall process performance. There are two possible explanations of the material removal mechanisms during CMP. One suggests that the work piece is separated from the polishing pad by a hydrodynamic fluid film (consisting of slurry) and the removal occurs due to the collision of the abrasives in the slurry with the surface. The other suggests that there is no hydrodynamic separation and that pad abrasiveness combined with slurry abrasives cause polishing. In both cases, a positive fluid pressure is expected at the interface [44]. During the first stages of research, fluid film thickness was found to increase with increasing platen speed and decrease with increasing load. The thickness of the film was found to be related to polishing rate, as a hydrodynamic lubrication layer. For permeable polishing pads (that have a mixed lubrication regime), the film fluid thickness varied little with either speed or load. CMP was also determined not to occur under a hydrodynamic lubrication regime because of the high permeability encountered, as well as the large pad roughness relative to the fluid film thickness [45]. It was later found that surface roughness of the pad due to conditioning results in negative vertical displacement of the polishing surface. Interfacial capillary forces were believed to account for most of the negative displacement at the time [46]. This negative displacement of the polishing surface was later found to be suction pressure at the wafer-pad interface. Finding subambient pressures under the polishing disk was counterintuitive at the time, but not at all surprising. A hydrodynamic lubrication flow mechanism, like a simple journal bearing, has both diverging and converging regions and sub-ambient pressures are observed in the diverging region. In CMP, it is possible to encounter such phenomena since the pressure (typical mean suction

pressure of 30 kPa) is well below vapor suction pressure of the slurry, and therefore no cavitation occurs. Increasing speed was found to increase suction pressure, while load had no distinct effect. Intuitively, with increasing load the thinner film incurs higher pressure [47]. The COF was also found to increase with speed, which suggested subambient pressures at the interface. Most importantly, it was also found that the COF also increased for a rotating wafer [4]. Further experiments were conducted using a steel puck with holes along its radius. The holes were connected to a pressure measuring device (piezoelectric transducers) through tubing and sampled one tube at a time, while the other cavities are kept sealed. Pressure maps were obtained by rotating the puck 45 degrees at a time. The leading 2/3 of the wafer was found to have sub-ambient pressures in the order of 50 kPa, and the trailing 1/3 of the wafer had positive pressures of approximately 10 kPa. Sub-ambient pressures will cause the silicon to be further impressed into the pad. The leading edge of the wafer was determined to "squeegee" the slurry at the interface, causing the sub-ambient pressure phenomena [48]. These findings are very significant for any CMP material removal model since uneven fluid pressures would affect the value of P (contact stress) in the previously presented Preston's equation. Contact stress is obtained by combining the effects of both applied normal load and interfacial fluid pressure.

Wafer polishing does not drastically deviate from polishing with a rigid flat surface. Suction pressure exists for plain and perforated IC100 pads, but not for groove pads. This difference is attributed to the grooves on the pad, which serve as a relief for the fluid pressure. The pressure magnitude with a wafer in place is higher

than those observed with a steel surface under the same conditions and this is attributed to the deflection of the wafer [49].

Since the sub-ambient fluid pressure is on the order of the wafer on pad contact stress, the total contact pressure is asymmetrical. Upon the discovery of these uneven fluid pressure distributions, further effort was targeted towards understanding how mechanical interactions caused by other parameters affected the magnitude of the interfacial fluid pressures. For most CMP conditions, the COF is between 0.2 and 0.5. As previously described, increasing speed increased the magnitude of the pressure, while changing load had little effect. The magnitude of subambient pressures was also found to increase with increasing surface roughness. Viscosity experiments demonstrated that the higher the fluid viscosity, the larger sub-ambient pressures exhibited. The effect of surface curvature on the fluid pressure is significant. With the surface changed from flat to 100 μm convex, the fluid pressure at the leading edge changed from sub-ambient to positive and almost zero at the trailing edge. The pad's elastic modulus was also determined to be a significant factor: an increasing elastic modulus resulted in a lower magnitude of sub-ambient pressures with almost no positive pressure in the trailing edge [50]. It was also determined experimentally that the pad exhibits viscoelastic properties, which allow it to compress under load. No sub-ambient pressures were observed until the pad was soaked for at least 24 hours, with increasing magnitude as soaking time increased [49].

Due to the success of the previous sets of experiments, new fixtures were designed and built to more accurately characterize the influence of pressure under certain conditions. One of the new fixtures had 20 pressure sensors aligned in the

tangential and radial directions, relative to the center of the pad. The sensors were directly mounted onto the fixture and data was read through a data acquisition cable which was connected to a data acquisition card and a computer. The purpose of this fixture was to measure interfacial fluid pressure in static mode without the time delay of the tubing used before [51]. The second fixture was designed for wafer bowing experiments. The fixture was designed to hold a wafer in place through the use of carrier film (as represented in Figure 2 found in page 3) with certain modifications. Holes were drilled into the fixture and punched through the carrier film to accommodate 8 capacity sensors in line from leading to trailing edge. The wafer's back was sputtered with metal and used as a target for the capacity sensors. Result of wafer bowing experiments displayed no noticeable speed or load effects, with little to no bending of the wafer. Wafer tilt was observed, evident by the carrier film compression [52].

The first modeling efforts for the subambient pressure phenomena were conducted by Levert [53] . He suggested a "suction cup" model in which the open pores of the pad acted as suction cup, creating subambient pressures at the interface. Johnson's contact model was used to explain the results, where the stress is higher near the edges of the contact zone. The contact stress in Johnson's model is defined by Equation 4

$$\sigma = \frac{P\cos(\pi\gamma)}{\pi\left(a^2 - x^2\right)^{1/2}}\left(\frac{a+x}{a-x}\right)^{\gamma} \qquad \text{Equation 4}$$

where

$$\cot(\pi\gamma) = -\frac{2(1-\nu)}{f(1-2\nu)} \qquad \text{Equation 5}$$

and P is the total load divided by the equivalent punch length, a is the radius of the wafer, and f is the coefficient of friction.

The contact stress is symmetric in static cases, but skewed in sliding cases due to friction. When the wafer first comes in contact with the pad, the asperities at the leading edge are compressed and the slurry entrained in this section is expelled. As the wafer slides across the pad, the reduction in contact stress allows the asperities to rebound and opens interasperity voids. This causes suction pressures to develop. The positive pressures at the trailing edge were then generated by the increase in contact stress which forces the slurry out of the interasperity voids. Levert suggested that Poiseuille flow explained the pressure distributions. Ng [54] modeled the deformation of the pad asperities using the Greenwood and Williamson equations for micro contact between a rough surface and a smooth plane, while assuming a Gaussian distribution for the asperity height distribution. Then the Navier-Stokes equations were reduced (using the continuity equations for mass conservation) to obtain a polar Reynolds equation to solve for the fluid pressure. The resulting Reynolds equation is described as

$$\frac{\partial}{\partial r}\left(rh^3 \frac{\partial p}{\partial r} \right) + \frac{1}{r}\left(h^3 \frac{\partial p}{\partial \theta} \right) = 6\mu \left[v_r \frac{\partial}{\partial r}(rh) + v_\theta \frac{\partial h}{\partial \theta} \right] \qquad \text{Equation 6}$$

which was solved by finite differencing. Then a force and moment balance was calculated to incorporate forces in the vertical direction and about the x and y axis. The results were later placed in a loop that checked for convergence and a final solution for the interfacial fluid pressure was obtained. Figure 3 displays a flowchart describing the process used to arrive to the final fluid pressure solution.

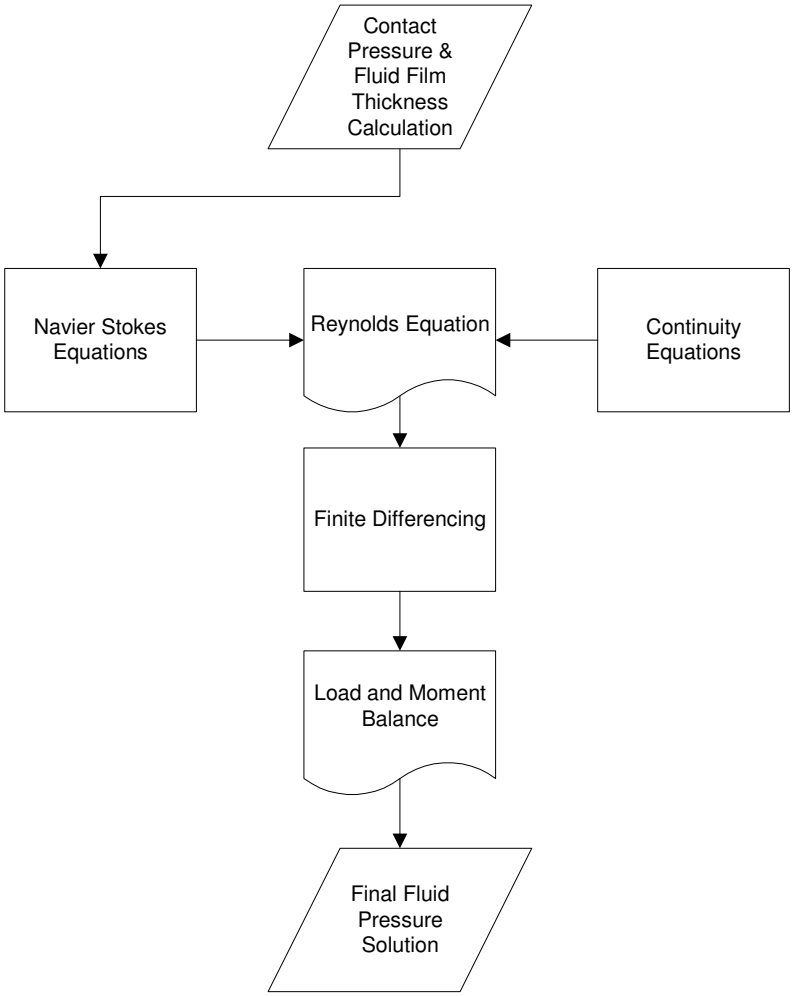

Figure 3. Flowchart of Interfacial Fluid Pressure Model

Data obtained from this computational model resembled static measurements, both in magnitude and location. The model was also able to predict changes with respect to speed and load applied on the wafer surface. An example of a comparison between the results measure experimentally and the modeled is presented in Figure 4. Part (a) displays the results obtained from direct measurements of the fluid pressure at the interface, while (b) shows the results obtained from the model after inputting the respective process parameters of the experiment. In these pressure maps, a region containing subambient pressures can be observed at the leading edge and a small region with positive pressures is observed at the trailing edge. These results are

typical for the experimental conditions used (non-rotating polishing head and conditioned plain pad).

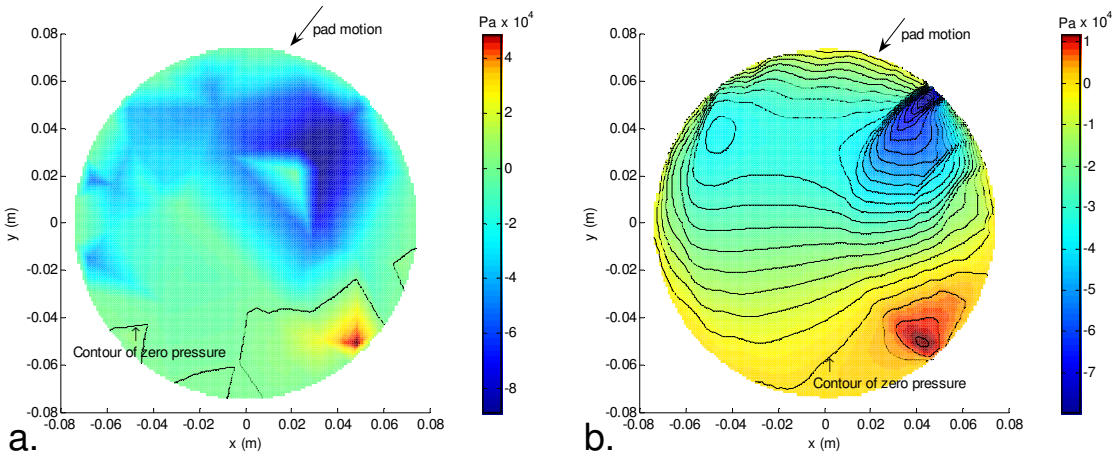

Figure 4. Comparison between Pressure (a) Measurements and (b) Model

CHAPTER 3
SYSTEM ARCHITECTURE AND DESIGN

Several devices were constructed through the course of this thesis for the purpose of measuring the effects of interfacial fluid pressure at the wafer-pad interface during CMP. These devices are composed of several components such as mechanical parts, electrical devices, and software, all designed in-house for user defined functionality. The different devices aim at obtaining information regarding the fluid pressure, temperature generation and variations, and wafer tilt of the wafer-pad interface during CMP. Device design details as well as software written to operate the devices or extract data are explained in this section.

Mechanical Devices

Three sensing mechanisms were used to measure pressure, temperature, and tilt through piezoresistive sensors, thermocouples, and capacitive sensors respectively. In addition, several mechanical devices were constructed for the purpose of housing these sensors and measuring interfacial fluid pressure, temperature changes, and tilt at the pad-wafer interface. Two fixtures made to hold sensors and one bridge assembly for tilt experiments were designed and built. One of the two fixtures was made using a rapid prototyping (RP) machine, while the second fixture was machined from a stainless steel puck. The schematic diagram in Figure 5a displays a top view of the RP fixture, which was fabricated in such a manner due to geometric complexities in the design. Figure 5b shows a cross-sectional view of the same fixture, marking the

angled cavities implemented in the design. The stainless steel fixture was designed to hold pressure sensors only, as well as serve as a target for the capacitive sensors used in the tilt measuring experiments. A schematic cross-sectional view of the steel fixture can be found in Figure 6. The bridge assembly (Figure 7) was designed to hold the capacitive sensors used in the tilt experiments with ample mobility and sturdiness. More detailed description of each individual system follows.

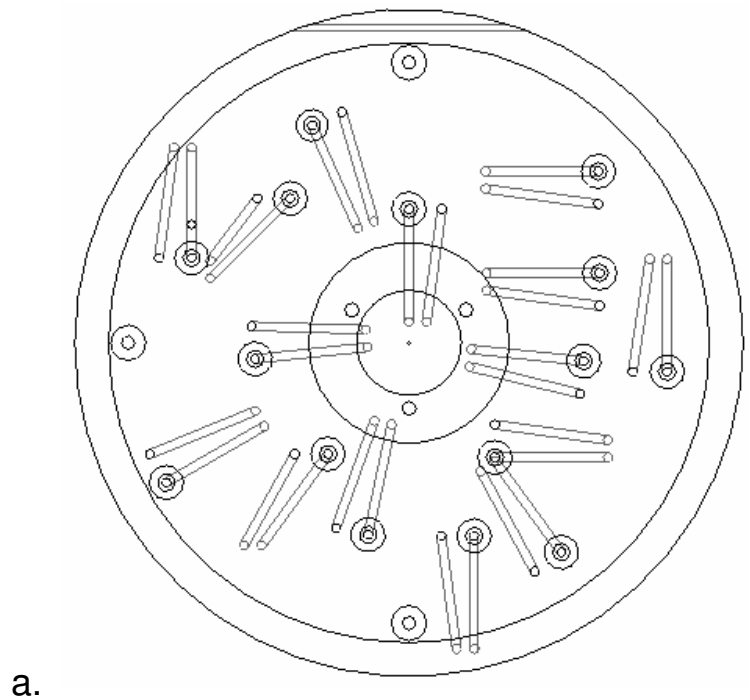

a.

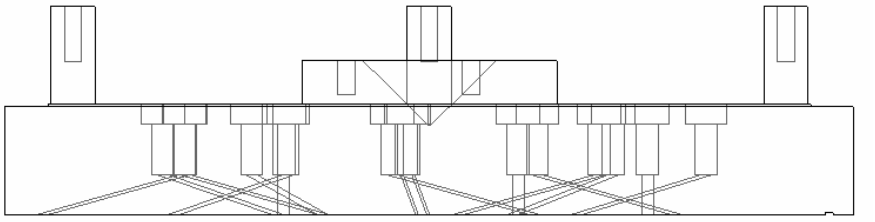

b.

Figure 5. Schematic (a) Top and (b) Cross-Sectional View of RP Fixture

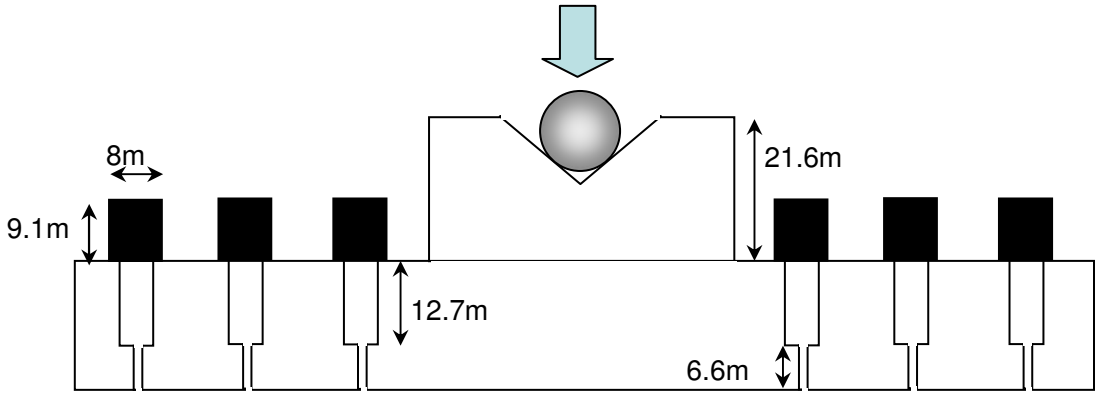

Figure 6. Schematic Cross-Sectional View of the Stainless Steel Fixture

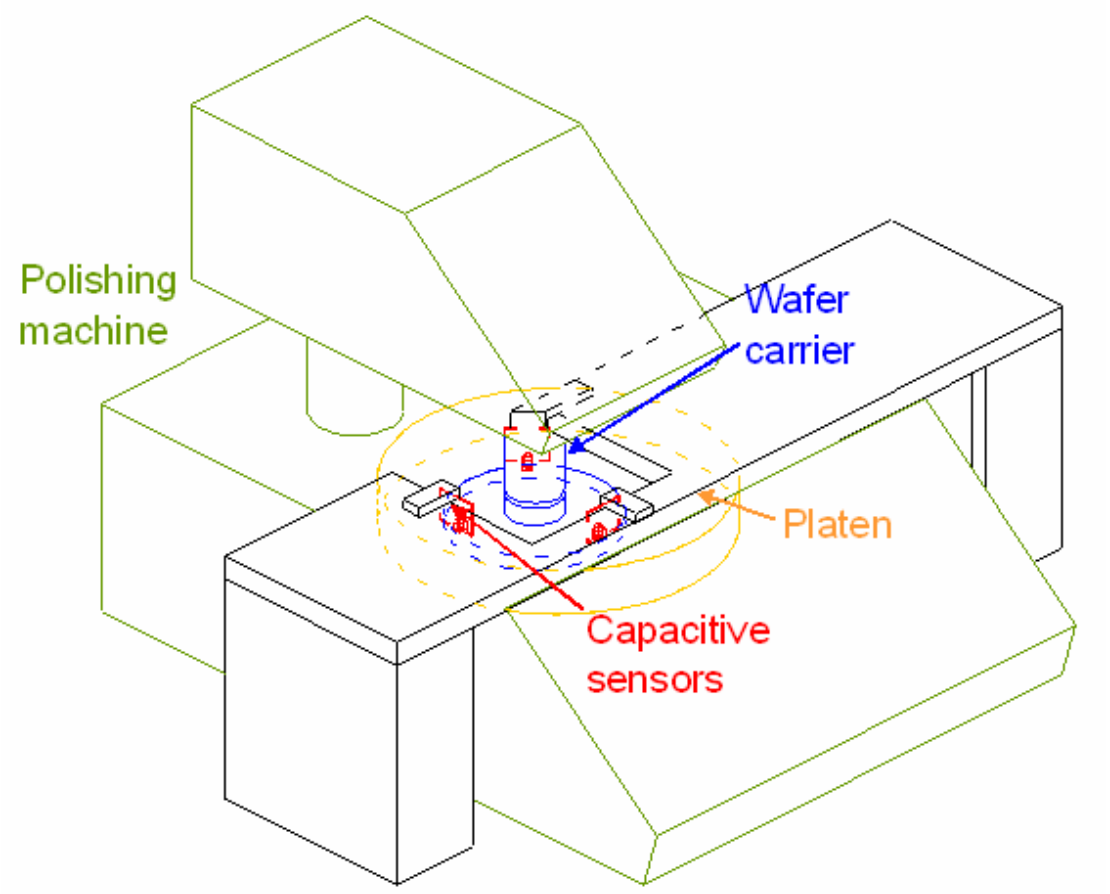

Figure 7. Schematic Diagram of the Bridge Assembly

Sensor Selection

The sensors selected to measure the various parameters of interest in this research were selected under various criteria: Input and output range, sensitivity range, accuracy, ease of use, and ease of installation. Various types and brands of sensors were reviewed and the following are the specifications of the selected sensors.

The pressure sensors selected were the 24PCCFH2G for the RP fixture and the 24PCCFA2G for the stainless steel fixture. These are piezoresistive membrane type transducers, both with very similar design except for their nozzle design. The RP fixture uses an M5 thread port while the steel fixture uses straight port, which was later threaded to fit a 12-24 NC tap. The most important characteristics of these sensors are their pressure range (-103 to 103 kPa) with a sensitivity of 2.175mV/kPa and their response time of 1.0 milliseconds. The sensors are also "ideal for wet/wet differential applications", which was another reason for their selection. The sensors are manufactured by Honeywell and further information regarding their operation information can be found in their catalogs.

The temperature sensors selected were copper/constantan wire type thermocouples from Omega Engineering, Inc part number 5TC-TT-T-30-36. These sensors are butt welded thermocouples with an operating range within the CMP expected temperatures and "good where moisture is present". They are also protected by a Teflon® insulating sleeve, making them "excellent" against solvents, acids, flame, and humidity. Thermocouples are also very sensitive and have a very fast response time. Further information regarding the operational information of these sensors can be found in Omega Engineering catalogs.

The capacitive sensors selected for the tilt experiments were obtained from previous setups at the EML laboratory. All three sensors were of the HPT-150 capacitive displacement type, having a maximum operating range of 2540µm. The sensors are very accurate within this range (± 0.2% linearity). The sensors and amplifying equipment are manufactured by Capacitec, Inc, and further information can be found in their product catalog.

RP Fixture Design

The first fixture built was the RP fixture. Its complex architecture was designed to serve three purposes: Hold pressure sensors for fluid pressure measurements, hold temperature sensors for interfacial temperature measurements, and serve as a target for the capacity sensors during tilt experiments. Fifteen pressure sensor cavities were designed to hold piezoresistive pressure sensors at distinct locations with respect to the center of the fixture. The purpose of this was to obtain maximum resolution as the fixture rotates during typical CMP conditions. All fifteen pressure sensor cavities were also designed to contain the same air volume to avoid any variations in sensitivity or response time. Sixteen temperature sensor cavities were also included in the design to house fifteen wire thermocouples. Fifteen of these cavities were placed at adjacent locations to the pressure cavities, while one cavity was left to measure the fixture's surface temperature (for control purposes). All fifteen pressure sensor cavities and temperature sensor cavities for interfacial measurements were designed as through-holes, and their locations were selected to avoid connectivity between the cavities and provide good spatial resolution. The through-holes were also at an angle to provide readings from underneath the fixture's

gimbaled joint, something not possible with straight through-holes. Table 1 below contains the coordinates of the exit holes for each sensor pair

.

Table 1. Coordinates of Exit Holes for Thermocouples and Pressure Sensors from RP Fixture's Bottom Side

Sensor #	X Pressure	Y Pressure	X Temp	Y Temp
1	4.76	0.00	4.76	-4.00
2	-0.99	9.47	2.98	9.89
3	-1.49	-14.20	-5.47	-13.79
4	-18.63	3.96	-17.80	7.87
5	15.93	-17.69	11.93	-17.43
6	26.10	11.62	27.73	7.96
7	-26.97	-19.59	-29.32	-16.35
8	-19.05	32.99	-15.58	34.99
9	19.13	-58.88	19.13	-54.88
10	14.71	45.29	18.71	45.29
11	-26.19	-45.36	-22.19	-45.36
12	-46.23	33.59	-46.23	37.59
13	39.15	-17.43	35.15	-17.43
14	44.61	49.54	44.61	53.54
15	-69.87	-14.85	-69.87	-10.85

The RP fixture is held to the arm of the polishing machine through a gimbaled joint, located at the center of the fixture. The gimbaled joint provides uniform loading to the fixture, while allowing it to accommodate to the profile of the rotating pad below. The bottom of the fixture was covered by a laser cut wafer. The laser cut wafer was cut from an 8-inch diameter wafer having p-type silicon in <111> crystal orientation. From this 8-inch wafer, a 6-inch round wafer (containing no distinctive flat) was obtained. Fifteen through holes located to match the location of the pressure sensor cavities were also cut, as well as fifteen blind holes with a 300µm depth for each temperature sensors. The blind holes were filled with thermally conductive paste and lined up with the pressure and temperature sensors, making sure that

thermocouple welds touched the silicon fixture. The wafer was later attached to the bottom of the fixture using a very thin (<200µm) double sided tape. A silicon ring was also cut from another similar 8-inch wafer. The ring's inside diameter was 5.5 inches and its outside diameter was 6 inches. The ring was then sputter coated with aluminum using a CVC Products DC sputterer located at the Georgia Tech Microelectronics Research Center (MiRC) cleanroom. The sputtered ring was placed on the upside of the fixture and served as a metallic surface target for the capacitive sensors in the tilt measurement setup, which is later described. Figure 8 displays a picture of the RP fixture from the top with all sensors labeled, while Figure 9 shows the bottom wafer with labeled exit holes.

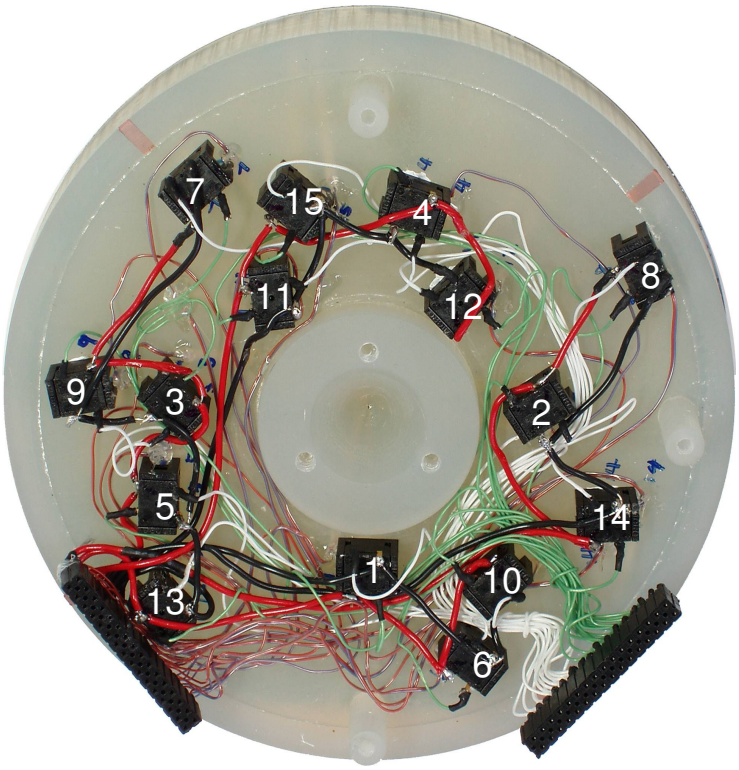

Figure 8. Top View Photograph of the RP Fixture

Figure 9. RP Fixture's Bottom Wafer

Several complications from this prototype were discovered at the time of implementation that did not allow it to serve all three functions. The first encountered complication was the fragility of the silicon ring and silicon wafer. The sputtered metal layer on the ring was easily subject to scratches which would affect the capacitive measurements. The ring structure itself was very fragile also, and broke within a few days. The wafer was very fragile also, especially at the positions where the through and blind holes were located. Another detrimental flaw in the design was the adhesive used to join the RP fixture to the laser cut wafer. The sealant was not strong enough to maintain pressure variations for the sensors to measure, which compromised the fixture's ability to report accurate results. To alleviate the situation, the wafer on the bottom of the RP fixture was replaced by a 6-inch wafer cut in a similar way, except only blind holes for the thermocouples were cut on the wafer's

back side this time. Also, no additional silicon rings were manufactured, leaving the RP fixture's functions limited to temperature sensing only. Later a stainless steel fixture was built to complement the RP fixture in its shortcomings.

Stainless Steel Fixture

The stainless steel fixture was constructed from a 6-inch type 303 stainless steel puck. First both sides of the fixture were faced on a lathe to achieve 2 parallel smooth surfaces. Then 15 through holes were drilled using a No 51 drill bit and a milling machine, in the positions exhibited by Table 2. These positions were chosen to maximize spatial resolution of data readouts and taking into consideration the size of the sensors to be mounted. Later, 2 sets of larger holes 0.2" and 0.3" in diameter were drilled and tapped to accommodate the sensor tips. A conical cut with a 90 degree tool was performed at the center of the fixture to accommodate a gimbaled joint fixture, which is used when attaching the fixture to the polishing arm of the CMP machine. Figure 10 shows a top view of the fixture, while Figure 11 shows the bottom through hole locations for the sensors as described on Table 2 (in a mirror image). Unfortunately, straight through-holes provide a blind area at the center of the wafer due to the gimbaled joint where no sensors can be mounted.

Table 2. Hole Positioning for Stainless Steel Fixture

Sensor #	X Pressure	Y Pressure
1	30.48	0.00
2	45.72	0.00
3	60.96	0.00
4	28.73	28.73
5	39.51	39.51
6	0.00	33.02
7	0.00	48.26
8	0.00	63.5
9	-41.30	41.30
10	-35.56	0.00
11	-50.8	0.00
12	-66.04	0.00
13	0.00	-38.1
14	0.00	-53.34
15	0.00	-68.58

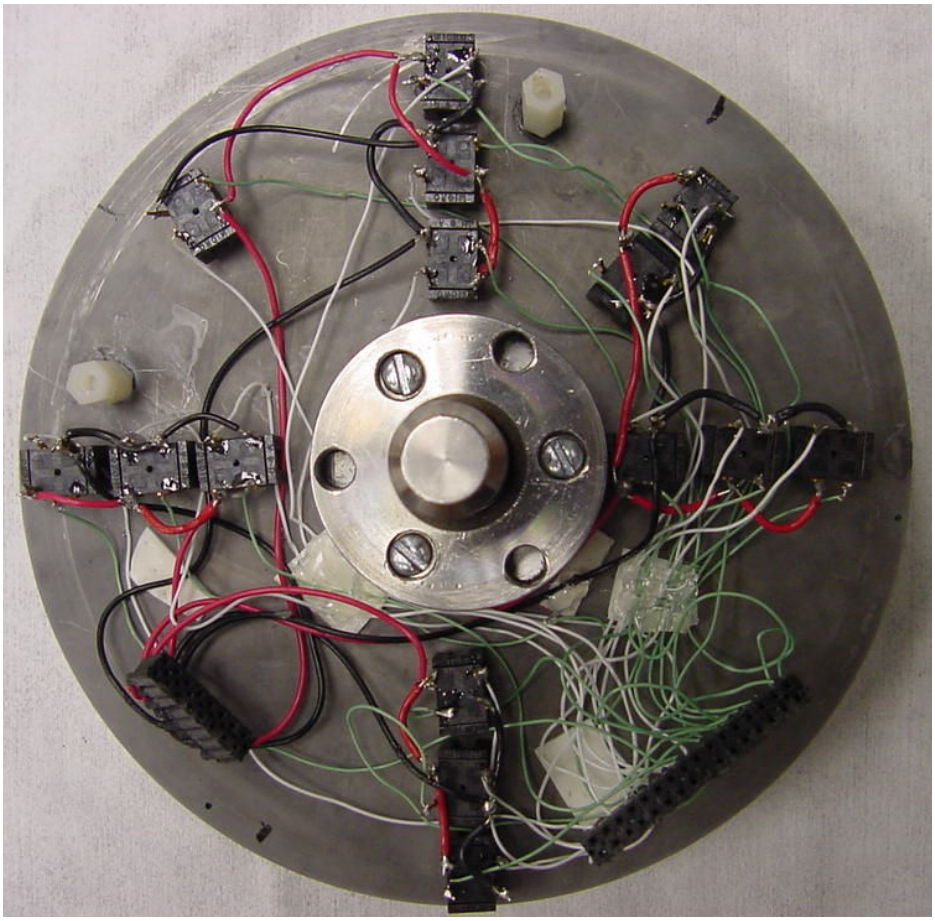

Figure 10. Stainless Steel Fixture Assembly

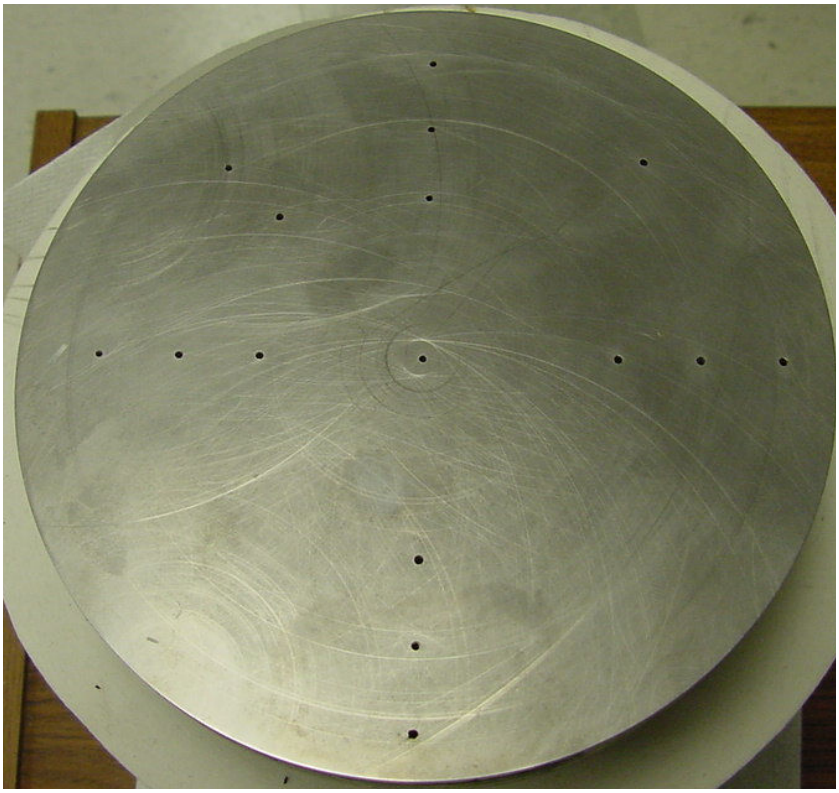

Figure 11. Bottom View of the Stainless Steel Fixture

After all the holes designated to hold the 15 pressure sensors were completed, the stainless steel fixture was sent to the Georgia Tech Research Institute's machine shop (GTRI) for precision lapping. Both faces of the fixture were lapped for several hours to obtain flatness from center to edge of around 5 µm. After the lapping process the sensor cavities were cleaned with compressed air and the sensors were put into position. A small track (about 6 mm wide) was purposely left uncovered by sensors to serve as a capacitive target during tilt experiments.

Capacitive Sensing Bridge

A bridge-like structure was built and designed to support three capacitive sensors used during tilt experiments. Each of the 3 capacitance sensors is held by a

rapid prototyped fixture attached to a micrometer for height adjustment purposes. The 3 micrometers are held within the center of the bridge structure by bolts attached to another larger rapid prototyped structure in the shape of a half square. This section is also securely bolted to the main stainless steel plate which comprises the main part of the bridge. The stainless steel plate is 30” x 10” in size and ¼” thick, and it is supported by 2 rolling beams that secure it to the 4 legs of the bridge. This architecture gives the bridge mobility in the x and z directions, which allows the user to comfortably place the bridge in place prior to experimentation, as well as adjust it for any experimental variations. The bottom of the legs is covered by a rubber film to dampen any outside vibrations during experimentation. Figure 12 shows the bridge structure at the sensor level, while Figure 13 displays the bridge structure at it’s testing position during an experimental run.

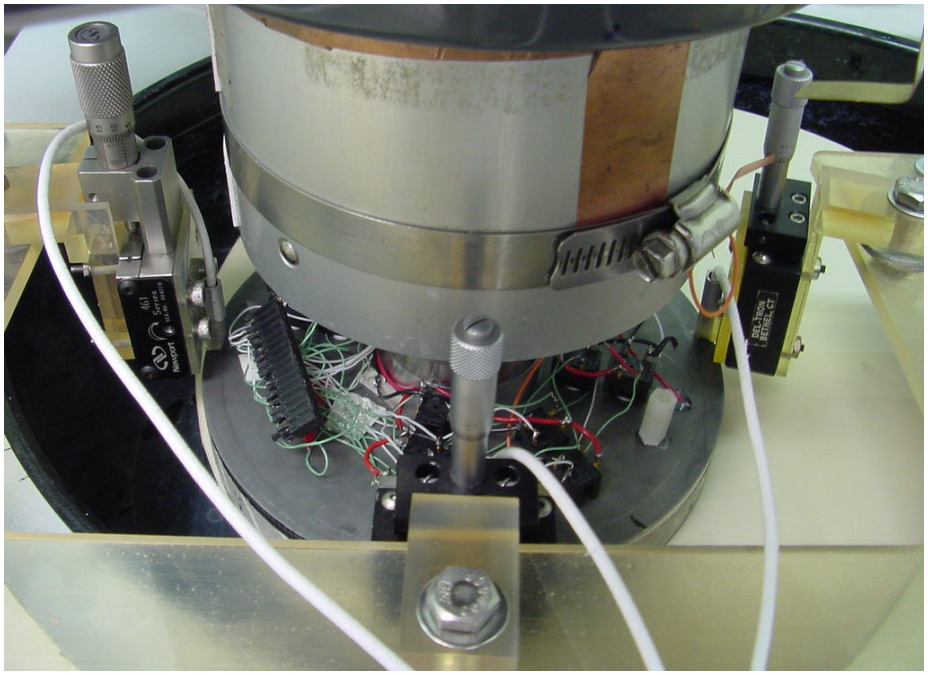

Figure 12. Bridge Structure Close-up

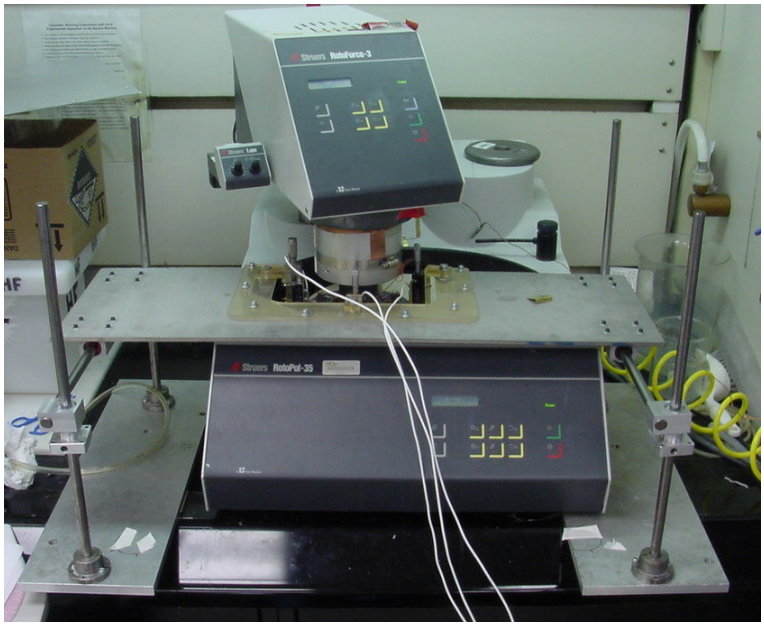

Figure 13. Bridge Structure Setup

Electronic Devices

Electrical components were used as part of a data acquisition system to receive data from the different sensors used in each setup (piezoresistive pressure sensors, thermocouples, or capacitive sensors). To acquire rotational data from the two fixtures containing the temperature and pressure sensors, a set of data transmission/data reception boards was assembled at the EML laboratory at Georgia Tech, specifically designed for this application. To acquire data from the tilt experimental setup, a set of amplifiers and a commercial data acquisition card were used. The following is a brief description of each of the different electrical devices implemented in this research.

Rotational Data Acquisition Transmission Board

A circular board was designed and built by S. Tsiareshka to sit on top of both fixtures and acquire data from the sensors mounted on them. This board then transmits the data through radio frequency (RF) to a receiver which then sends the data to the computer for further analysis. A photograph of the transmission board can be seen in Figure 14. Different components on the board have been grouped to display their main function.

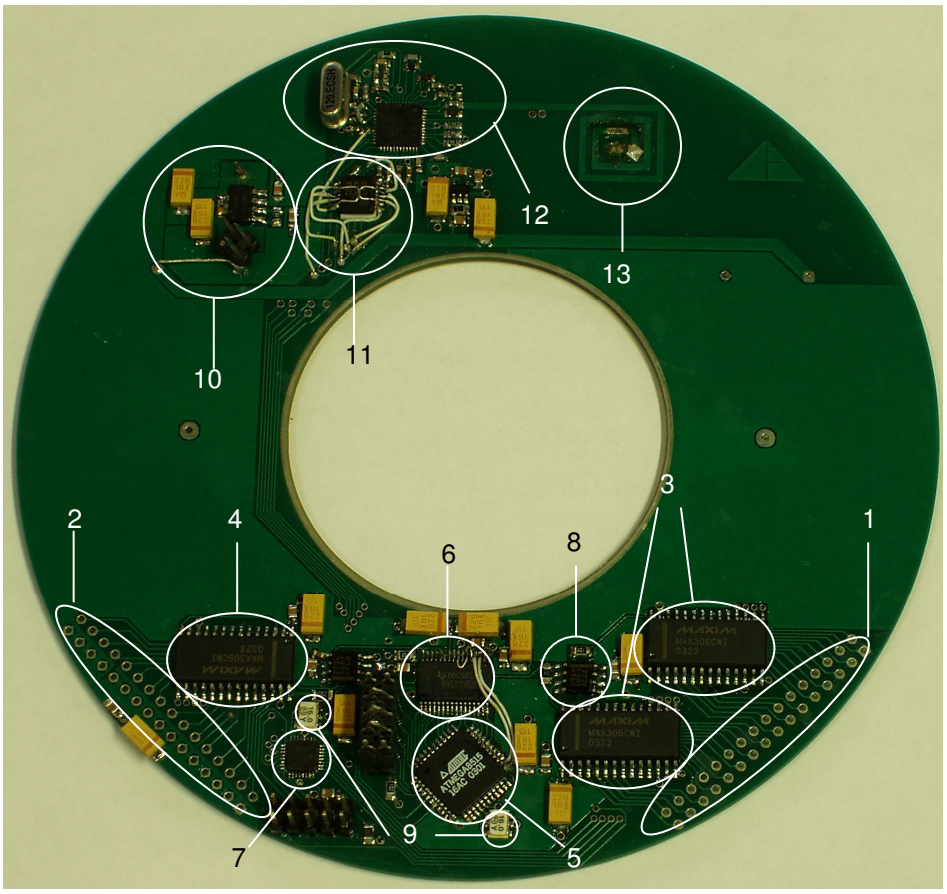

Figure 14. Transmission Board Layout

Section 1 is the pin configuration that is directly connected to the pressure sensors. There are 32 available pins: 15 are connected to the positive terminals of the pressure sensors, 15 are connected to the negative terminals of the pressure sensors. Section 2 is the pin configuration that is connected to the thermocouples and the power for the pressure sensors. It too has 32 available pins: 16 connected to the positive terminal of the thermocouples, 8 connected to the negative terminals of the thermocouples (2 thermocouples per pin), and 8 supply 5V to the pressure sensors (4 positive and 4 negative terminals). Section 3 is the multiplexers (MUX) for the pressure sensors. Each MUX has 16 channels and cycles through the sensors in a specified patterned dictated by the microcontroller on the board. Section 4 is the MUX for the thermocouples and it functions in a similar way. Section 5 is the board's microcontroller. This chip is the unit's main control, dictating acquisition, reading outputs from the analog-to-digital converter, and sending them to the transmitter. The microcontroller is also programmable through a set of pins adjacent to it. Section 6 is the analog-to-digital converter (ADC). This unit transforms the analog signals transferred from the pressure and temperature sensors into digital signals. Section 7 is the MUX controller, which initializes acquisition and selects the channels from the MUX to be sampled. Section 8 is the pressure sensor amplifier. Section 9 displays the clocks, which are used by the system for timing. Section 10 is the power converting unit. Power from batteries (around 6V) is converted to 5V and 2.5V, which are used by the devices on the board and by the pressure sensors on the fixture to function. Section 11 is the logic level 2.5V-5V converter, which allows communication between two units powered by different voltages. Section 12 groups all the

components which make up the transmitter. Section 13 is the system's antenna, which currently uses a resistor to transmit digital data to the data receiver board. A data acquisition flowchart for this system can be seen below.

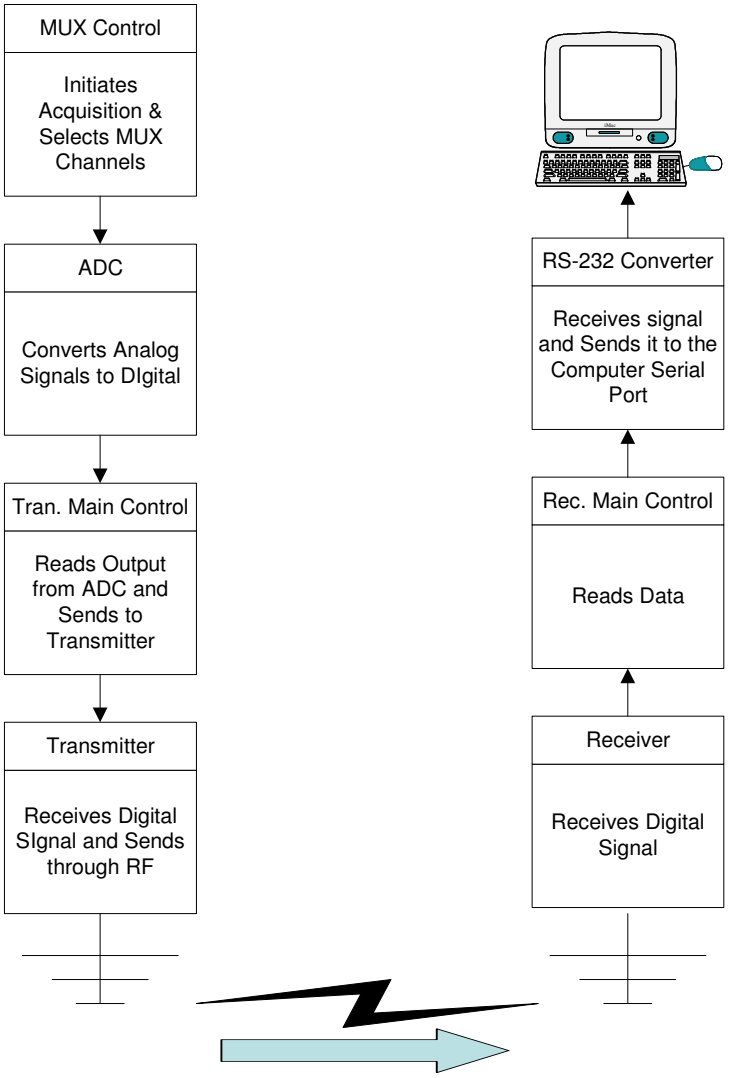

Figure 15. Data Acquisition Flowchart

Data Acquisition Receiver Board

A rectangular board was also designed and built by S. Tsiareshka to receive all data transmitted by the transmission board and inputting this data into the computer. A picture of the receiver board can be seen in Figure 16. In this picture the main components of the receiver unit have been grouped for further explanation.

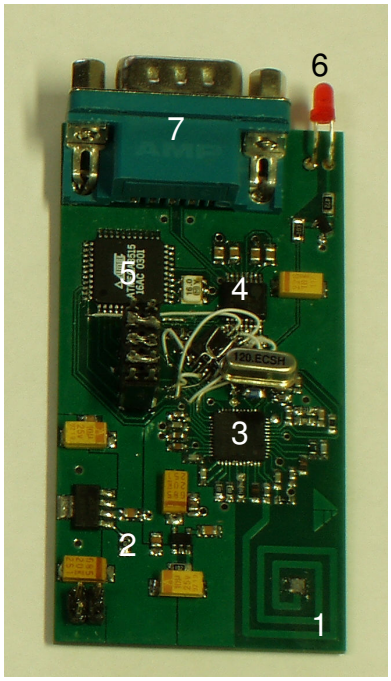

Figure 16. Receiver Board Layout

Section 1 shown in Figure 16 is the antenna. As in the transmission board, the antenna utilizes a resistor to obtain the digital signal. Section 2 is the power conversion unit, which converts the input power of 6V into the appropriate voltage used by the various components. Section 3 is the receiver, which much like the transmitter has its own clock to time signals and a processing unit. Section 4 is the RS-232 Interface controller, which converts TTL logic signals into signals for the

serial port (RS-232). Section 5 is the main processing unit, which controls the data reception and flow throughout the system. The device enumerated number 6 is a light emitting diode (LED) which illuminates in case of active connection. Part 7 is the RS-232 port or COMM connection, where the receiver sends the acquired data to the computer's COMM port through cable for analysis.

Capacitive Sensing Amplifiers and DAQ card

The capacitive sensors data acquisition system also requires several electronic devices to transfer analog readouts performed by the sensors to the computer for analysis. First, each of the sensors is connected to an amplifier card (4100-SL) from Capacitec to amplify the signal. The three amplifiers can be individually adjusted, but have a common clock and power source of 15V coming from a 4100-B card. After the signal is amplified, each individual output from the amplifiers is transferred to the computer by a National Instruments PCI-6071E DAQ card and board using three differential channels. The board is connected to a data acquisition card connected to the computer via cables. A photograph displaying the amplifiers and the input board with cable connection can be seen in Figure 17.

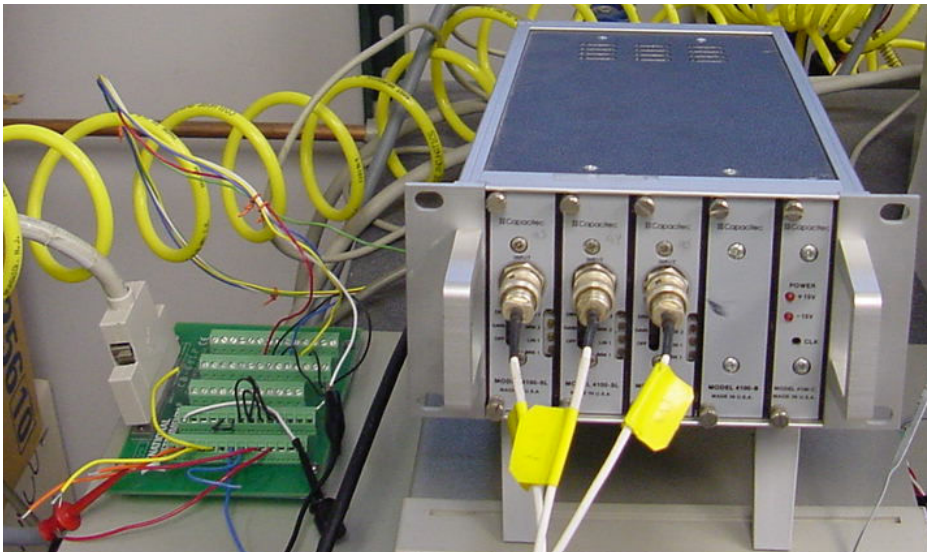

Figure 17. Capacitive Amplifiers and Input Board

Software Architecture

Several software programs were written to operate the data acquisition devices or to manipulate the acquired data for analysis purposes. The following is a description of the software used.

Pressure and Temperature Sensing Software

Various programs were written to acquire and manipulate data coming from the rotating fixtures. These types of programs are intended for data acquisition from the various devices used, while a second type of programs was coded to analyze the incoming data. A series of programs were coded to dictate the behavior of the electronic components on the data acquisition and transmission boards for the rotating fixtures. These program files were written in C programming language and controls processes via the microcontrollers. It also dictates data acquisition sequence (of the sensors) and changes sampling rate of the card. The software that controls the data

acquisition from the capacitive sensors was written in LabView (from National Instruments). It controls the incoming data from the data acquisition card installed in the computer. LabView programs also provide a graphical user interface for the user to test signals and monitor measurements while the system is running.

The second set of programs was designed for data analysis of the rotating fixtures. All data analysis software was written in Matlab. This code is able to take a data stream of bits from the output file from the computer, decode it into real signal measurements, organize it in matrix form, and plot it corresponding to the angle of rotation and differential pressure or temperature reading. Imbedded in the code are all calibration measurements and coordinate information necessary to output a 2D map of what the sensors measured while in rotation. The program uses the first 4 revolutions of the fixtures, which occur in the air, as the zero point for temperature and pressure and then measures the difference in signals to compute a change. It also sets up boundary conditions and plotting scheme. The algorithm is structured to plot any desired revolution, with all the analyzed data from that revolution properly located at the sensor's location when measured. Examples of sensor mapping for the pressure and temperature fixtures are displayed in Figure 18 and Figure 19 respectively. The origin marks the center of the fixture with the center of the pad to the right of it, as displayed in the diagrams. The number of data points per sensor in one revolution depends on the sampling rate of the data acquisition board, which is controlled by the microcontroller. In the current setup, a 1000 hertz frequency is used. This frequency provides for approximately 25 cycles throughout the 32 sensors in one revolution and determines the sensor mapping coordinates seen below.

.

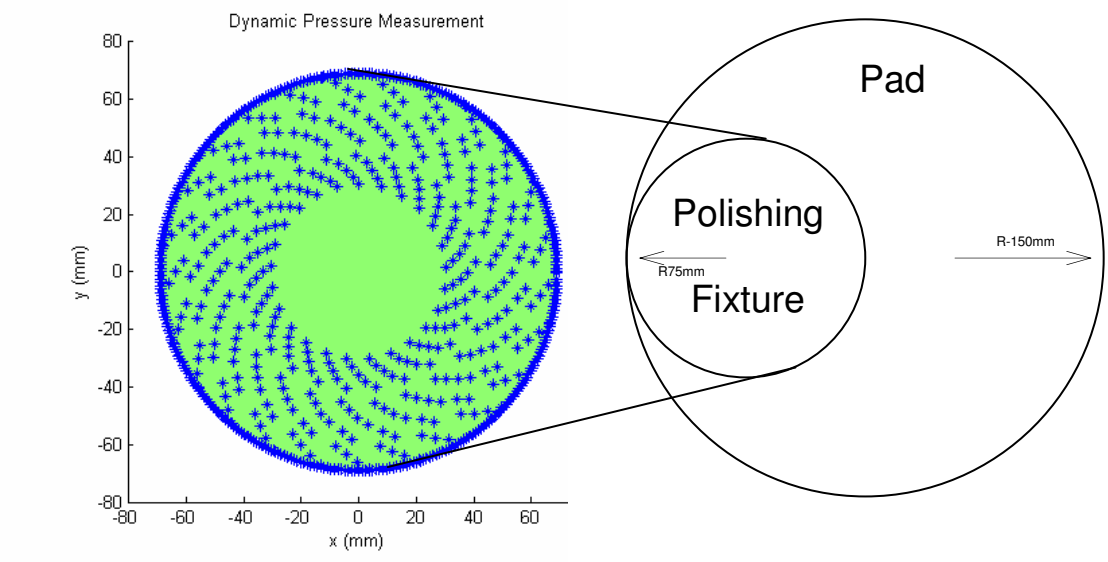

Figure 18. Pressure Sensor Mapping

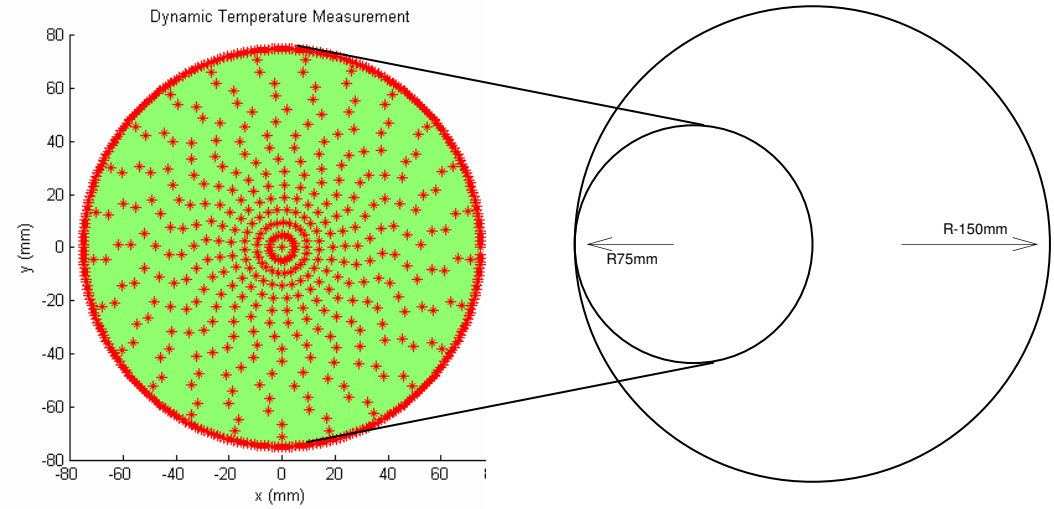

Figure 19. Temperature Sensor Mapping

Other programs in Matlab were later designed to filter signal noise, obtain relative speeds, and serve other purposes outside of data manipulation. All data manipulation and calculations for the capacitive sensors is performed through the use of spreadsheets and therefore no algorithms were coded for its analysis.

CHAPTER 4
SYSTEM CHECK AND CALIBRATION

This section describes calibration setups and results, equipment modifications and conditions, device testing and results, and signal noise reduction efforts.

Device Calibration

The sensors and devices were then calibrated to determine calibration curves, sensor response, and assure accuracy and reputability of the results. The first sensors to be calibrated were the pressure sensors, then temperature sensors, and finally the capacitive sensors. The polishing machine's rotational speeds were also checked for accuracy purposes. The procedure and results of all device calibrations follow.

Pressure Sensors Calibration

The pressure sensors were calibrated using various techniques to insure the maximum accuracy of the readings. It is important to note that the pressure sensor tables provided by the manufacturer show a linear behavior within their operating range, the output being proportional to the voltage applied. The manufacturer specifications suggest a change in output signal of 2.175mV/kPa at a nominal input voltage of 10V. The first set of calibrations performed used a vacuum pump to apply a suction pressure of around 33 kPa to each sensor. Results for these calibrations are displayed in Table 3. The small deviation in the readings can be attributed to the seal used between mounted sensors and the air hose from the pump, which is not perfectly

hermetic. Also, the pump's analog gage is hard to read accurately and can sometimes fluctuate in a range of about 1.5 kPa.

Table 3. Pressure Calibrations at Varying Voltages with 33kPa Applied Suction

Sensor #	6V	8V	10V
1	-4.83	-5.07	-5.11
2	-4.64	-5.01	-5.01
3	-4.91	-4.97	-4.94
4	-4.27	-4.68	-4.69
5	-4.96	-4.90	-4.81
6	-4.53	-4.86	-4.82
7	-4.86	-4.87	-4.81
8	-4.76	-4.83	-4.89
9	-4.77	-5.04	-4.93
10	-4.79	-4.79	-4.71
11	-4.88	-4.98	-4.93
12	-4.62	-4.83	-4.71
13	-4.78	-4.98	-4.94
14	-4.44	-4.90	-4.87
15	-4.50	-4.58	-4.52
Average	-4.70	-4.89	-4.85

A different set of calibrations was conducted to check for the sensor order output of data acquisition card. This experiments checks for both the correct sensing order as coded into the board's microcontroller, the correct column alignment in the plotting algorithm, as well as the provide a basis for data regression from the data input signal to the card's output signal. This test is conducted using the same vacuum pump, this time by checking the sensors in order. The results in Figure 20 show the sensor output throughout the experiment. Each sensor is represented by a color and all 15 sensors responded when a vacuum is applied. Every sensor has its own offset, which is later subtracted from the results by the plotting algorithm. The vertical lines on the bottom of the figure the signal from a light interrupter whose purpose is later

explained. All units are arbitrary and therefore not displayed. Figure 21a shows the sensor's offset at 5V as transmitted by the data acquisition card, while Figure 21b displays the same offset when read manually with a multimeter. This offset is used to calibrate the amplification done by the card and determine the real signal value. A Linear regression between both parameters was implemented, yielding a multiplication factor of 15.32 with an R-square of 97%. This result provides confidence regarding the data transmission with regards to pressure sensors.

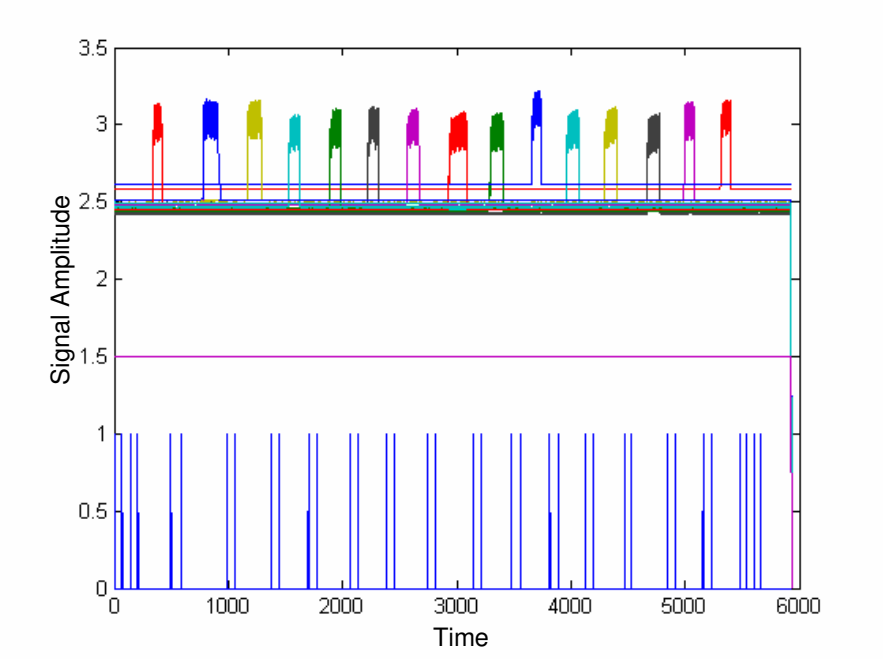

Figure 20. Sensor Order Check

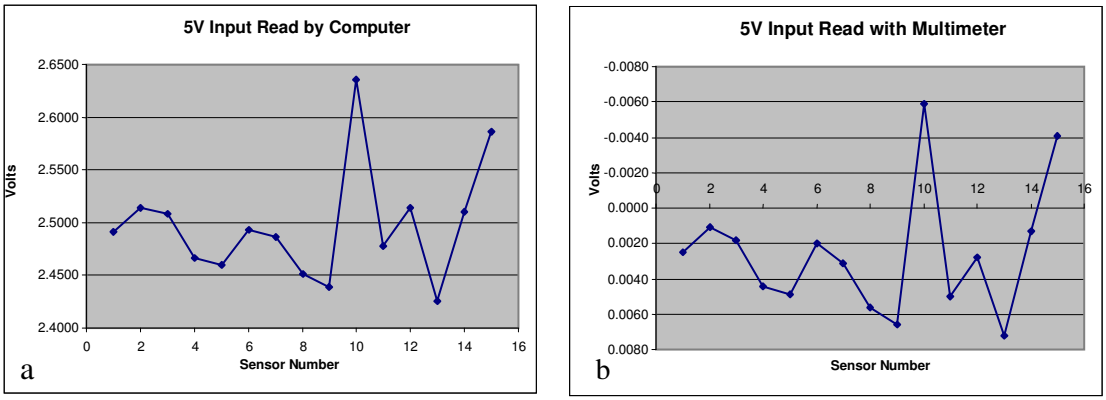

Figure 21. Sensor Offset as Measured by (a) Computer and (b) Manually

Temperature Sensors Calibration

The temperature sensors were also calibrated to ensure their linearity and proper functionality. Ample amounts of literature can be found regarding the specific thermocouples used and the manufacturer provides response charts and calibration tables suitable for different applications. This calibration data was corroborated by the use of a hot plate and water, while the sensors were inside the RP fixture and in contact with the silicon wafer below. Figure 22 shows a photograph of the actual temperature calibration setup where water in a metal container was heated from -5^{o}C to 55^{o}C and readings of each thermocouple were taken at various temperature stages. Two thermometers were used in the setting, one to measure the water temperature (temperature of the silicon wafer), and one to measure the temperature of the thermocouple ends. The difference of the two is the effective temperature change sensed by the thermocouples. This temperature change was then correlated to the output voltage of the thermocouples to produce a temperature calibration curve for each sensor.

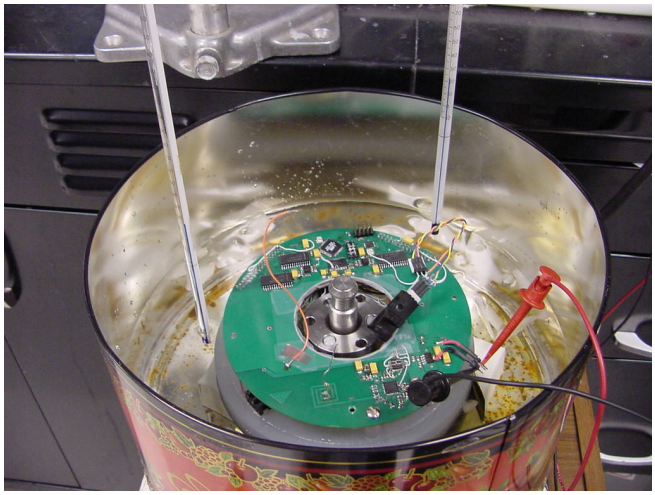

Figure 22. Temperature Calibration Setup

Several repetitions of this temperature calibration procedure were conducted, yielding very good repeatability. The temperature sensors were found to have slightly different slopes and offset and therefore individual calibration curves for each sensor were coded into the plotting algorithms. The data was interpreted as linear with an average R-square of 98%. Figure 23 is a sample of the data used in the regression models to obtain calibrations curves. It can be noted that sensor 5 is a little off, the reason being that this sensor is the one located inside the RP fixture and is only used for checking purposes, not during the plotting.

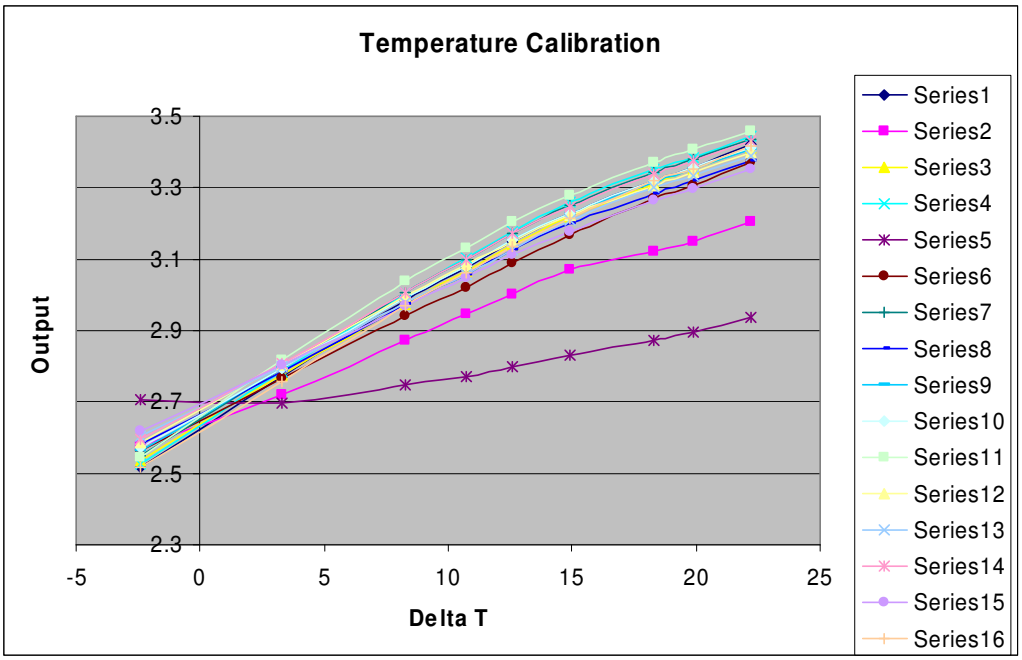

Figure 23. Temperature Calibration Data Used during Regression

Capacitive Sensors Calibration

Capacitive sensors were calibrated following the calibration instructions found in the Capacitec Operational/Maintenance Manual. The first step was setting the amplifier cards to the right setting. This was done by turning the dial screws for the drive, gain, and offset functions to the appropriate levels (as indicated in the manual). The next step was to produce calibration curves for each sensor with their corresponding amplifier card. This was achieved through the use of a micrometer on a stage with an orifice for the capacitive sensor to lay at rest. The micrometer was then grounded to the same ground as the amplifier cards and moved towards the capacitive sensor until it touched. The output voltage was offset to 0 using the offset dial on the amplifier cards. Then the micrometer was moved away from the capacitive sensor, one thousands of an inch at a time. The value at each location was recorded until the

total displacement was 762 microns. The data was then put into the LabView program to change the output from a voltage reading to displacement in microns. Figure 24 shows a sample calibration curve obtained from sensor 2. As it can be observed, the sensors' output is very linear with respect to separation from the target.

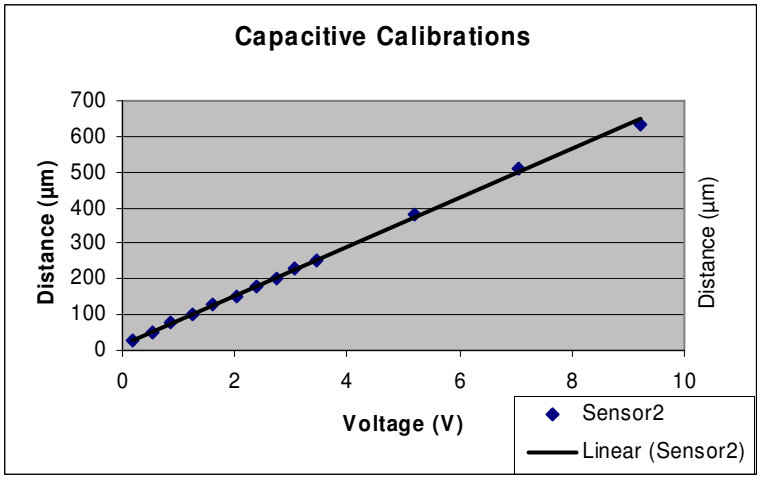

Figure 24. Capacitive Sensor 2 Calibration Curve

Accuracy and Response Time

The pressure sensor's response time was checked by rotating the fixture in the air while applying compressed air (positive pressure) at a specific point in the fixture. This experiment was also useful to check the sensor positioning performed by the mapping algorithm and the sensitivity of the sensors. Results are displayed in Figure 25, where in part (a) compressed air was applied directly on a sensor at 45 degree angle from the pad's center, while in (b) air was applied on a sensor at a 200 degree angle from the pad's center. The air duct was very close to the fixture's surface in experiment (a), as can be seen by the magnitude of the signal. In experiment (b) the

hose was about 5mm away from the surface. Different sensors were tested with similar results. The results of these experiments show that the sensors have very little delay, if any, when measuring pressure evolutions in rotational cases. It also shows that there is no connectivity between them and the fact that in some cases 2 sensors can pick up on the air stream at different magnitudes is very encouraging.

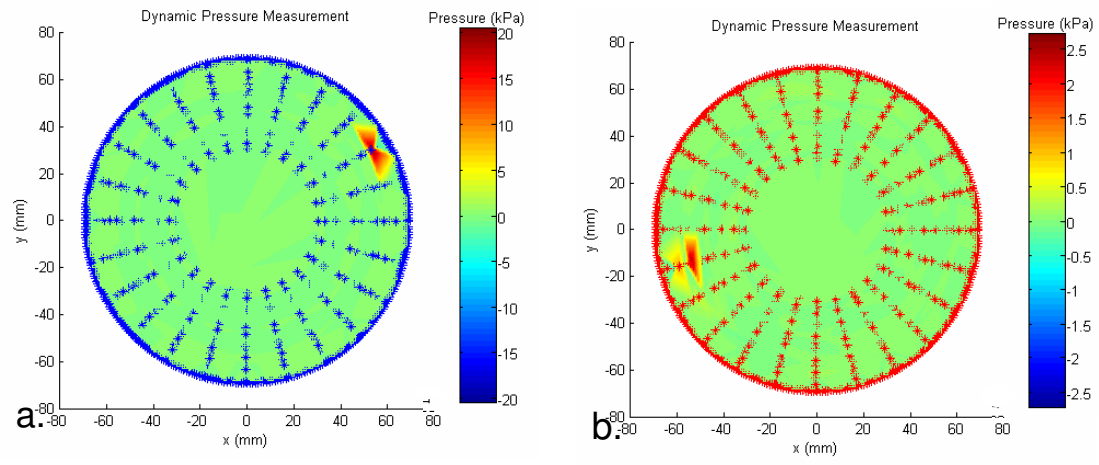

Figure 25. Rotational Testing Using Compressed Air at (a) 45° and (b) 200°

Another similar test was performed, this time during lubricated contact with the polyurethane pads. To try and obtain distinct readings from the fixture, 3 circular patterns were cut into the pad (with around 100 µm depth) at 3 angular positions with respect to the fixture. The pad was then soaked with water and placed on the platen of the polishing machine. Some conditioning with a diamond disk was necessary due to some protrusion of pad particles above the mean surface of the pad that lifted during the cut. The pad was not rotated, while the head rotated on top of the designed patterns. The results showed that the sensors could clearly measure subambient pressures at least 2 of locations where the voids were and some traces of a third. The

results are not perfect due to the crudeness of the setup and the possible tilt of the fixture due to uneven surface profiles caused by the deformed pad. Results can be observed in Figure 26.

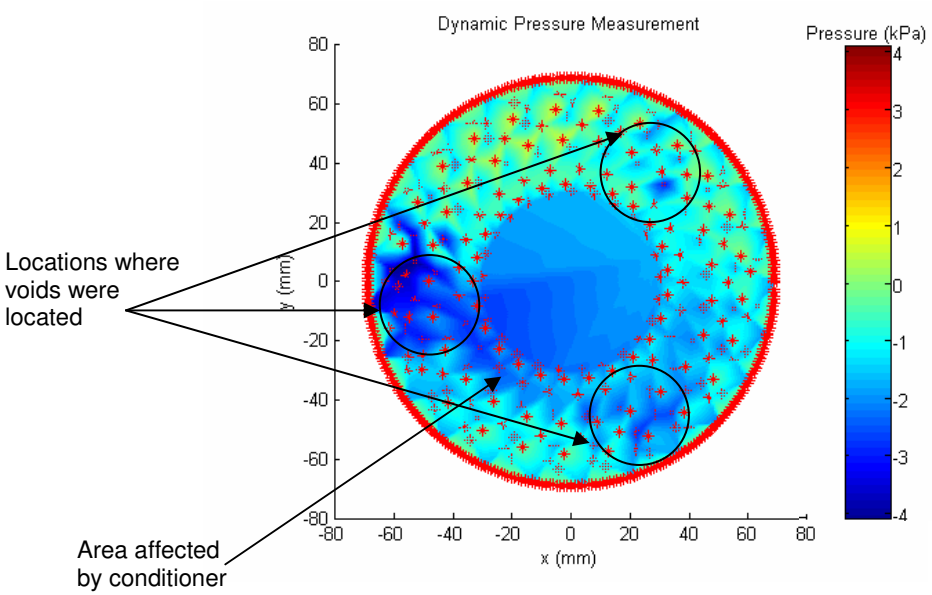

Figure 26. Patterned Pad Results

To test the frequency response and time delay that the wireless card could potentially introduce into the readings, a waveform generator was used. The waveform generator was set at different frequencies, different voltage amplitudes, and different wave patterns to test the effective time delay of the wireless board. The outputs of the waveform generator were connected to the card as inputs (as if they were a sensor producing the signal) and then the output was obtained and plotted. All test resulted in positive results, suggesting that the acquisition and transmission board running at a 1000Hz frequency is able to sample and transmit points at an almost immediate pace. Figure 27a shows a diagram of a square wave with 10mv amplitude

and 5Hz frequency which was set as an input. Figure 27b shows a close up of a wavelength, where one wavelength was captured by 12 points on the plot (1000Hz ÷ 5Hz ÷ 16 sensors). Similar results were obtained when using a sinusoidal and a triangular input at various frequencies. It is important to know that when reading these graphs and any other similar graph for pressure sensors, an increase in signal signifies negative gauge pressure, while a decline in signal signifies positive gauge pressure. Results for temperature measurements are consistent with the y-axis (a rise in temperature is represented by a rise in output signal).

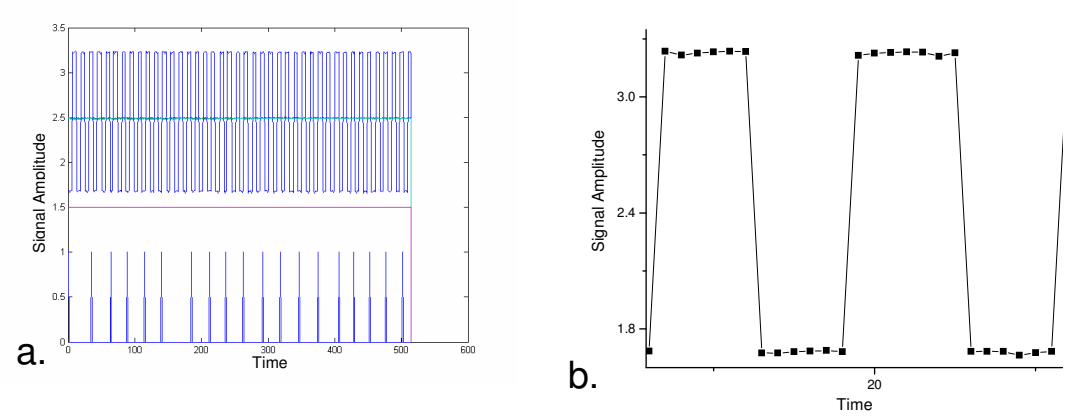

Figure 27. Sampling Frequency and Data Transmission Test

Noise Reduction and Control

Several actions were undertaken to reduce the noise observed in the signals. Most of the noise observed was electronic noise created by the various motors and electronic devices that surround the fixture. Mechanical noise was also observed in the capacitive measurements due to a possible wobble of the polishing platen and

unevenness of the targeting surface. A description of the changes to the original setup or mathematical computations used to control noise factors follows.

Fixture Grounding

The first source of electrical noise encountered was found to be very detrimental to the rotating fixtures' accuracy. After much searching for the source of the noise, it was determined through oscilloscope readings that the polishing arm and the polishing pad carried very strong 60hz noise, which was later introduced into the fixture. Electrical charges from both sides were creating a "capacitor effect" on the fixture. The sensor outputs would pick up that input during the analog stage, which was then converted into a digital signal and transmitted over RF. To minimize the source of noise, the polishing machine was partially disassembled and two 2 Amp leaf type carbon brushes were placed on the top motor's spindle and on the rotating platen (which is attached to the pad). Both of these carbon brushes were wired to the electrical outlet's ground. This change in the setup reduced the background noise over one order of magnitude, from around 20mv to less than 2mv. The dramatic improvement in signal to noise ratio can be observed in Figure 28 below. Figure 28a shows a readout of the pressure sensors during an experiment prior to grounding, while Figure 28b shows a readout of the same fixture during a post-grounding experiment. The signal in part b is much cleaner and this results in more accurate data plots.

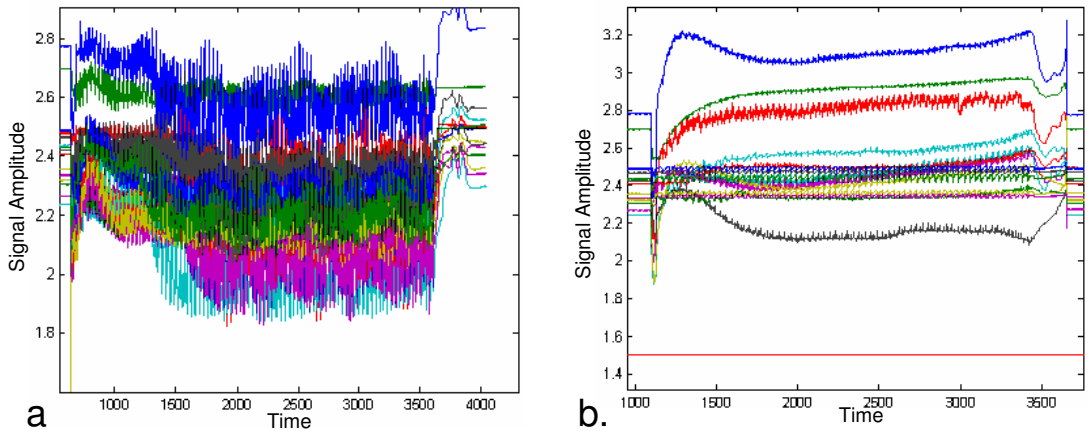

Figure 28. Grounding Effects on Signal to Noise Ratio

Another source of signal noise is the grounding of the circuit board itself. Since the data acquisition board is rotating with the polishing arm, it was not effectively connected to any effective ground. This created a problem in which the board would sometimes produce spikes in the data, which were not part of the readings. These spikes were also detrimental to the plotting algorithm, since they get plotted with the rest of the data if the user is unaware of their existence. The existence of only one signal spike in the data of a particular revolution effectively ruins the possibility to display the data accurately and therefore renders hundreds of real data points useless. The data spike phenomena affects both pressure and temperature measurements. The first step towards eliminating this effect was to ground the rotating board to the same ground as the platen and arm motor. This was done by placing an adhesive copper film around the circumference of the polishing arm and soldering a wire from this copper strip to the fixture. A copper wire was then looped around the copper strip to act as a "slip ring commutator" and connected to ground. The addition of this additional ground greatly improved the spike problem, but not

completely solved it. The number of spikes was decreased by over 80%, but still some remained. This is due to the occasional skip of the loop from the copper track, which immediately causes a spike. The problem was later corrected though the implementation of a filtering algorithm.

Software Filtering

Various sources of noise were filtered by using algorithms. As previously discussed, the spike phenomena was not completely removed by the grounding of the rotating board. A filtering algorithm was then implemented to filter the remaining spikes through the use of tolerance levels for changes between consecutive data points. This method proved to be very effective at eliminating most if not all of the remaining spikes, as well as providing an indication of which revolutions in data might be heavily influence by spikes and should not be used. An example of a heavily spiked data plot which was treated with the filtering algorithms is displayed in Figure 29. The data plot on the right is the result after filtering. One can appreciate from the plots that the data did not change for any of the sensors measured, the only difference is the removal of the spikes in the data.

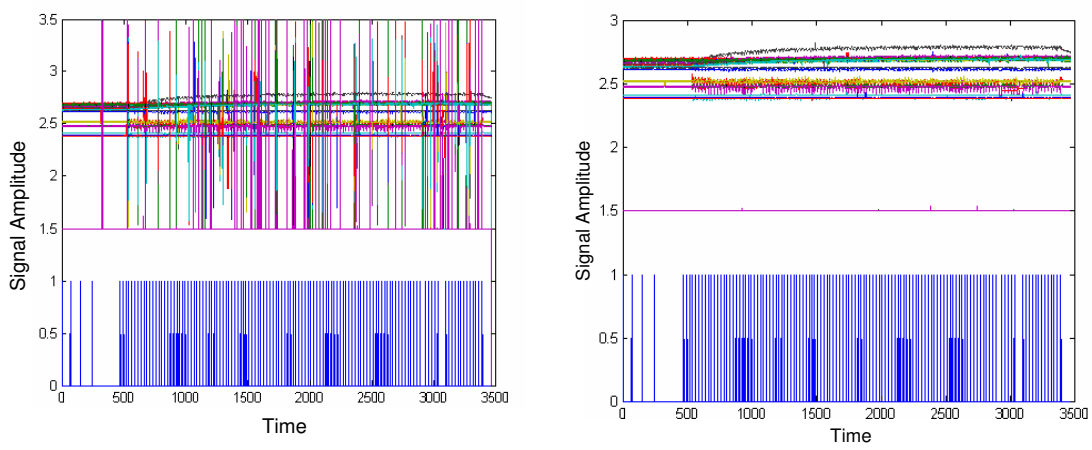

Figure 29. Filtering Algorithm Effects on Spiked Data

A different data filtering scheme was used to filter mechanical noise from the capacitive sensing setup. The two sources of noise in the capacitive sensing setup are the wobble of the pad and the unevenness of the target. As previously described in chapter 3, the target (the upside of the steel fixture) was lapped to a very high level of flatness. Unfortunately through the course of sensor installation and experimentation, several scratches occurred on the top surface of the fixture, affecting the track used during capacitive sensing. The noise filtering in this case was done in spreadsheet form by using various equations and tolerance measures to find measurements at the exact same point in both the pad and the fixture. This way displacement is measured without the influence of either the pad or the capacitive track variations. An example of the data obtained by the capacitive sensors is shown in Figure 30, where it is possible to observe both the variations due to the track (small oscillations) and the pad's wobble (long oscillations).

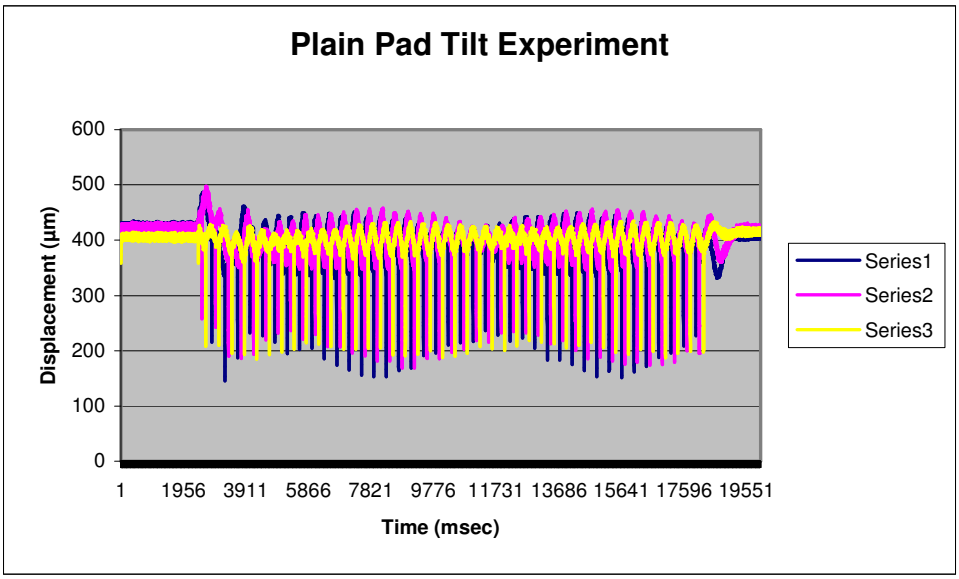

Figure 30. Tilt Experiments Noise Source

CHAPTER 5

EXPERIMENTAL SETUP

This section describes the experimental setup used while running the pressure, temperature, and tilt experiments. Include in this section are experimental variables studied in the experiments, as well as information regarding controlled parameters which were kept constant throughout the experiment.

Experimental Variables

One of the main purposes of this research is to dynamically measure the interfacial fluid pressure and temperature (response parameters) at the wafer-pad interface. Various conditions were altered through the course of the experiments to observe how various process parameters affect the magnitude and distribution of set response parameters. Among the variables studied were the pad's surface profile, slurry type, and slurry flow rate. Important polishing parameters such as velocity and normal load were not extensively studied due to the amount of previous research and understanding of that area at the EML laboratory [54][55].

Polishing Pads

Three pads were used during all experimental setups. The pads used were an IC-1000 k-groove pad, an IC-1000 unconditioned (new) pad, and an IC-1000 conditioned pad with a purposely set topography. This pad's profile was severely changed by using a lathe with a carbide cutting tool and later refined by the use of a

diamond impregnated conditioning disk. All three pads were then soaked for several days prior to use to stabilize water absorption and the pads' elastic and shear modulus. Profiles of the pads were scanned with a profilometer, using three overlapping scans to compile a complete line scan of the pad. The profiles were measured in several directions to insure the pad's uniformity along all radial directions. The surface roughness was also measured since it has been proven to influence the material removal rate mechanisms during CMP. Figure 31 describes the way in which the three surface profiles had to be measured due to the length of the pad being used. These profiles were then stitched together in the following fashion: First the center scan was leveled. Then the overlapping portions of the scan (3 cm in each direction) were fitted using linear regression. After, the left and right portions of the scan were rotated and translated to fit in with the center scan. Finally, a 249 point moving average is used to estimate the mean surface of the pad and produce a 30 cm diametric scan.

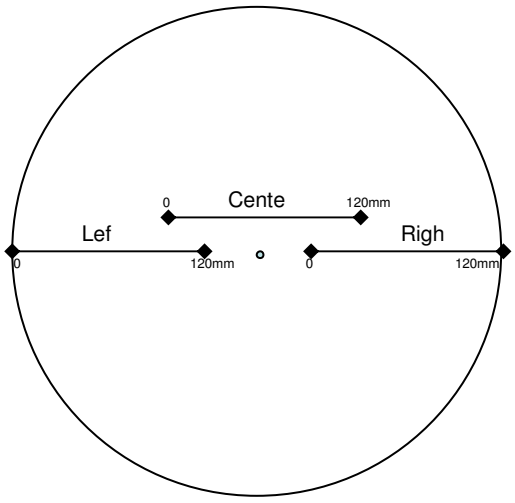

Figure 31. Profilometry Scan Technique for the Pads

The roughness of the k-groove pad was not determined due to the channels on the pad. The average roughness (R_a) of the unconditioned pad was consistently under 3 µm, while the R_a of the conditioned pad varied from 6.5 to 8 µm.

Figure 32, Figure 33, and Figure 34 on page 70 display profile results from the 3 pads being utilized. The first diagram shows the profile of the k-groove pad. The grooves on the pad are not displayed since the profilometer's tip used was larger than the size of the grooves. This was done intentionally to measure the profile of the interface between the pad and the fixtures, not just the profile. The center to edge variation in the k-groove pad is about 20-25 µm. The second diagram on the page shows the profile of the unconditioned pad. This profile was measured using the same tip radius and resulted in a center to edge variation of about 5 µm. This result is not surprising for plain unconditioned pads, which are supposed to be very flat in nature. Pad break-in processes, as well as material removal and conditioning will deteriorate the new pad's profile under normal polishing conditions. That is why the third pad was purposely conditioned, to analyze the effects of pad changes during CMP. The third pad was measured in the same manner as the two previous pads and displays a 35 µm center to edge deviation. Results presented later show how this small change in geometry has enormous effects in the pressure, temperature, and tilt evolution during polishing.

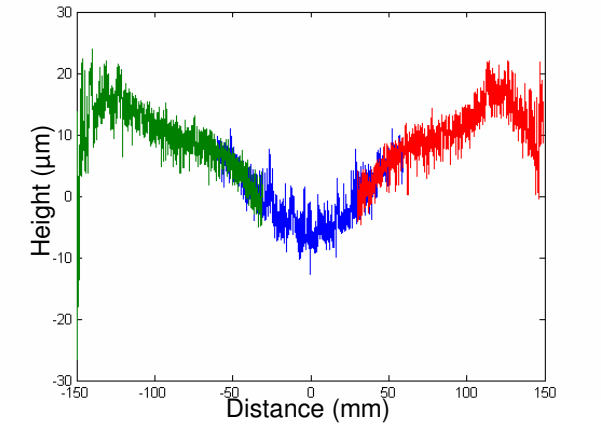

Figure 32. Global Interface Profile of the K-Groove Pad

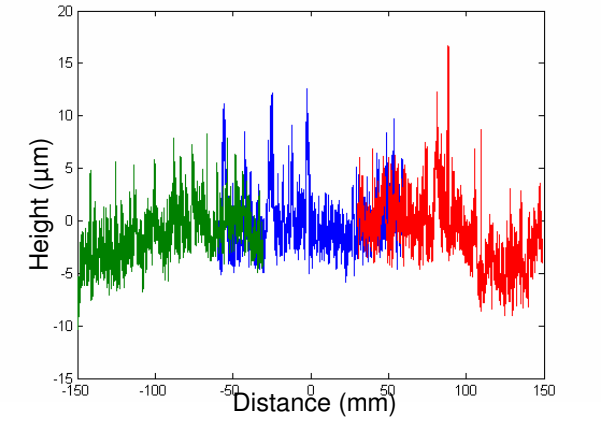

Figure 33. Global Interface Profile of the Unconditioned Pad

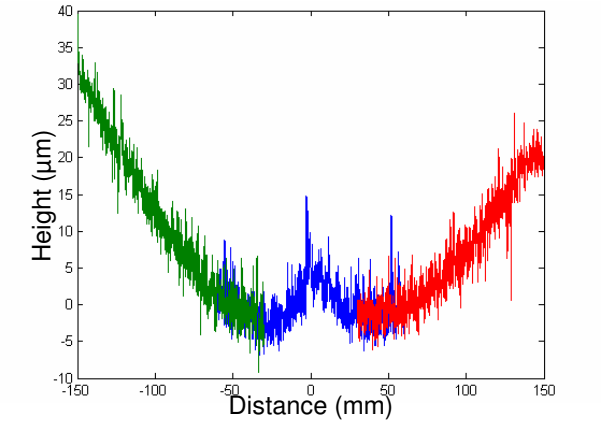

Figure 34. Global Interface Profile of the Conditioned Pad

Slurry Flow

Slurry flow is a very important parameter for this type of CMP studies, especially since it serves as the only form of lubrication between the pad and the polishing fixture. Slurry flow rates were carefully controlled to provide a good indication of slurry effects at the interface. The slurry was delivered by a Masterflex L/S peristaltic pump from Cole Palmer Instrument Company. The flow rates used were carefully selected to avoid slurry starvation of the CMP process and close to commercial polishing processes. The slurry was delivered by tubing to a location prior to the contact between the pad and the fixture, the slurry was allowed to spread about the pad by centripetal forces. The location of the fluid delivery varied with respect to the flow rate in an effort to deliver a uniform amount of slurry across the wafer. The slurry used for the temperature experiments was a commercially available hydrogen peroxide silica particle slurry from EKC Technology, Inc. On the other hand, for pressure measurements water was used instead of slurry to avoid scratching or oxidizing the polishing surface or clogging the sensor holes. The flow rates used were 60, 100, and 140 ml/min.

Experimental Setup and Changes

Once the various devices were built and tested, the experimental setup was put together. This section contains information regarding several components, not part of the polishing machine or the rotating fixtures, which had to be added. It also discusses the final setup assembly and the procedure to run the various experiments.

Additional Components

Several additional components were added to the original setup to serve various functions. One of these components is power supply to both the data acquisition/transmission board and another to the receiver. The receiver was powered by a standard DC power supply set at 6V. The transmitter is powered by 4 AA rechargeable batteries mounted on the polishing arm (which rotates with the board and provide 6V of DC power). Also mounted to the polishing arm is a photointerrupter, which is directly connected and powered by the transmission board. This photointerrupter signals when a complete revolution has been completed, which resets sensor channels for a new rotational sequence measurement. Essentially, the signals from the interrupter are embedded into the code and used by the data acquisition system and software to know the exact location of all sensors at any point in time. The rotating interrupter utilizes a stationary brass sheet (mounted onto the polisher) to trigger signals.

Pressure and Temperature Experimental Setup and Procedure

With all the components ready and calibrated, the polishing setup was put together. First the complete rotating system is put together. The rotational board was placed on top of the fixture and the sensor connection blocks were connected to the inputs on the board. Figure 35 shows a picture of the stainless steel fixture when it is completely assembled, ready to be place under the polishing arm. In this picture one can see: (a) the board securely bolted on top of the fixture, (b) the sensor connection blocks, (c) the photointerrupter connection, (d) the power connector, and (e) the grounding wire which grounds the board to the polishing arm.

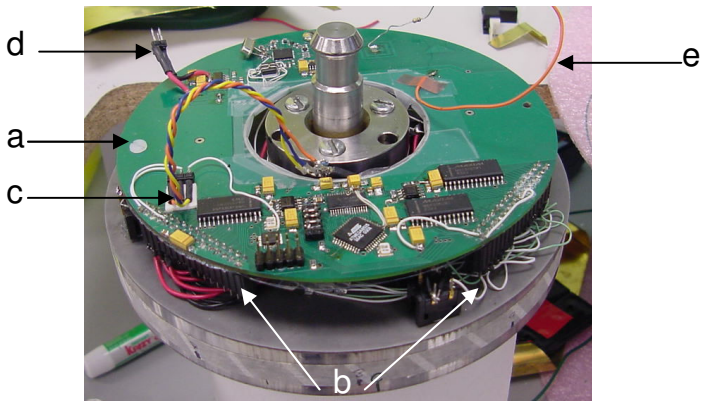

Figure 35. Rotating System Complete Assembly

The next step is to securely place the fixture under the polishing arm. After this, all the peripheral systems are connected: The receiver board is powered and the RS-232 interface is connected to the serial COMM port of the computer. The photointerrupter is then connected to the rotating board. The grounding wire is attached to the polishing arm and all grounding connections are tested for connectivity. The polisher used is a RotoPol-35 bench-top polishing machine from Struers with platen speed range of 40-600 RPM variable in 10 RPM intervals. The attached polishing arm is a RotoForce-3 also from Struers with set 150 RPM rotational speed and a load range of 30-400 N adjustable in 10 N intervals. The pressure is applied via a pneumatic arm and is continually being monitored and adjusted by the equipment. The platen containing the pad is placed inside the polishing machine and the speed and load parameters are set. The slurry pump is started at the desired flow rate and the data acquisition software is initialized. The pad is then rotated while the fixture stays in its original position. The photointerrupter is manually triggered 4 times for zeroing purposes (as explained in the "Pressure and Temperature Sensing Software" section) and the polishing fixture is finally rotated

and brought into contact with the pad. It is important to know that the polishing head does about 3 full revolutions in the air before coming in contact with the pad, which is evident in the plot results. Figure 36 shows a photograph of the polishing setup used to measure the temperature and pressure. In the picture we can see (a) the slurry reservoir, (b) peristaltic pump, (c) bench-top polisher, (d) polishing arm (rotating part), and (e) polishing arm controls. Figure 37 shows a close-up photograph of the same polishing setup. In this picture we can easily observe (f) the polishing pad, (g) the polishing fixture, (h) the transmission board, (i) the batteries, (j) the interrupter, (k) the stationary interrupter plate, (l) the copper strip (for grounding), (m) grounding connections from the head to the pad, and (n) the slurry outlet.

Figure 36. Complete Polishing Setup

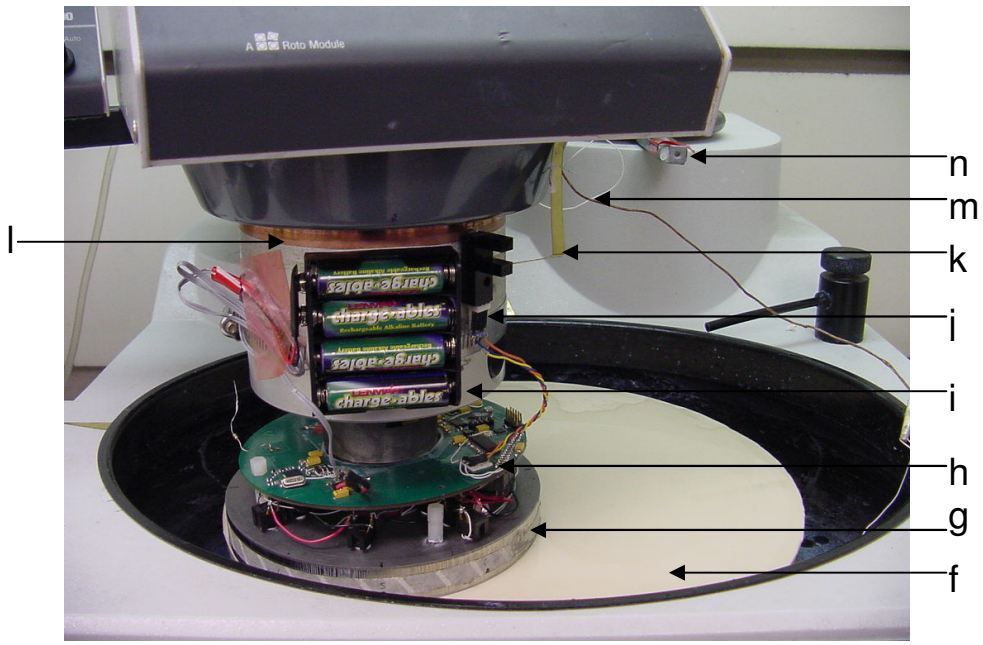

Figure 37. Complete Polishing Setup Close up

After the desired data has been collected, the polishing process is stopped, and the data acquisition is terminated using the software interface on the computer. The file containing the results for the polishing measurements is then transformed from bits of data to real signal measurements by the preprocess.m script, which then places the data in matrix form (each column of the output matrix represents a particular sensor). The file is then processed for plotting through the use of the Dynamic.m function in the case of pressure measurements or the SiDynamic.m function in the case of temperature measurements. Spikes in the data can be eliminated by using the SSpike.m script for pressure measurements or the SiSpike.m script for temperature measurements.

Tilt Experimental Setup and Procedure

The capacitive setup is used to measure the fixture's tilt when it comes in contact with the polishing pad. The tilt measured is generated by the pad and fixture rotation, which is caused by the shear stress moment on the polishing fixture and total contact stress distribution created by the relative motion at the pad-fixture interface. Prior to the experiments, the track on the stainless steel fixture which serves as a target for the capacitive sensors was cleaned and cleared of any obstacles that could jeopardize the integrity of the system. A very thin piece of single crystal silicon with a thickness of around 140 µm was place on the track to serve as signal "interrupter" to determine the position of the disk during data analysis. The first step putting the tilt experiments setup together was to place the assembled capacitive bridge setup at its proper location with regards to the polishing equipment. Figure 13 on page 43 shows a picture of such location. The second step was press the fixture down onto the pad, without any rotation of the pad or the fixture. Once the fixture is down, the capacitive sensors are moved into position and graduated to about 400 µm from the surface of the fixture. Figure 12 on page 42 shows a picture of the sensor level setup position. The position of the sensors is then recorded and the target is grounded to the same ground as the capacitive sensors. Then, the data acquisition software is initialized and the pad and fixture rotations are started simultaneously. The samples per channel were set to 20,000 at a sampling rate of 1000Hz, which equates to 20 seconds of data per experiment for all 3 channels. To calculate tilt, the relative position of the sensors to the target is important, as well as the angle between them. It was also important to define two angles and one displacement value that describe tilt and to formulate

equations to find these parameters. The first angle, θ or azimuth angle, is used to describe the angle between the general x axis and the position where the fixture is at its lowest point of contact. The second angle, φ or tilt angle, describes the angle between the general z axis and the vector normal to the surface of the fixture. The third parameter, dz or lift, shows the vertical displacement of the fixture. Figure 38 shows a graphic representation of the azimuth and tilt angles.

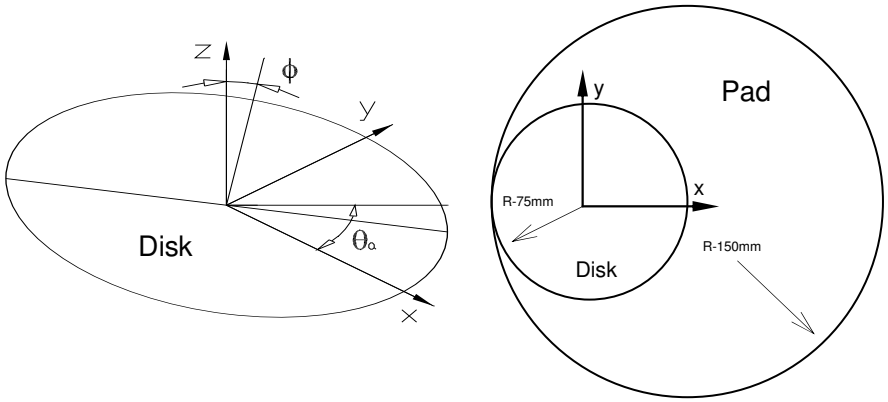

Figure 38. Azimuth and Tilt Angles' Definition

By measuring the positions at which the sensors are located with respect to the fixture, we can calculate the tilt parameters. The first step is to calculate vectors between sensor 1 and 2, and sensors 2 and three. By cross multiplying these vectors (which lay on the same plane), we can find the vector which is normal to the plane. The unit normal vector is then found by dividing this vector by its magnitude. From here, all parameters can be obtained using the following geometric relations:

$$\theta = \pi + a\tan\left(U_{ny} / U_{nx}\right) \qquad \text{Equation 7}$$

$$\phi = a\cos(U_n \bullet U_z)$$ Equation 8

$$dz = \frac{\left[(x_1 \times U_{nz}) + (y_1 \times U_{ny}) + (dz_1 \times U_{nz})\right]}{U_{nz}}$$ Equation 9

where U_{n*} is the unit normal and its components, U_z is the (0,0,1) vector, and x_1 y_1 and dz_1 are the x y coordinates and displacement for sensors 1. These equations were coded into a Matlab program to provide tilt results from the data read by the capacitive sensors. Results and discussion of the pressure, temperature, and tilt experiments follows.

CHAPTER 6

RESULTS AND DISCUSSION

Multiple experiments were run with the rotating fixtures to perform in-situ analyses of the pressure and temperature distributions at the wafer-pad interface. The tilt generated by the contact stress distribution and shear stress moment was also studied, as well as the effects of pad geometry and slurry flow in the response parameters. Some calculations regarding important rotational components are also presented.

Relative Velocity Calculations

The relative velocity between the pad and the wafer is a very important parameter in the CMP process. Velocity is one of the components of Preston's removal rate relation (see Equation 1 on page 4), Reynolds equation (derived from the Navier-Stokes system of equations) which determines hydrodynamic fluid pressures, and determines Couette and Poiseuille flow fields. The velocity of the pad-wafer interface changes depending on the relative position of the pad's and fixture's center and the angular rotation of the pad and fixture. Equation 10 relates the velocity component of every point on the wafer-pad interface

$$V_f = \sqrt{V_r^2 + V_R^2 - \left[V_r \times V_R \times Cos(\pi - \alpha)\right]} \qquad \text{Equation 10}$$

where V_r and V_R are the velocity components due to the fixture's and pad's rotation respectively, and α is defined by the relation

$$\alpha = Sin\left(\frac{d-x}{R}\right) - Sin\left(\frac{\| x \|}{r}\right) \qquad \text{Equation 11}$$

where d is distance between the center of the pad and the center of the fixture, x is the x coordinate of the point (with the pad center as the origin), and R and r are the Euclidean distances from the point to the center of the pad and the fixture respectively. A velocity map representing a static fixture and a rotating pad of similar size and configuration as the polishing setup is displayed in Figure 39. It is important to note that the fixture rotates counterclockwise in the same direction as the pad.

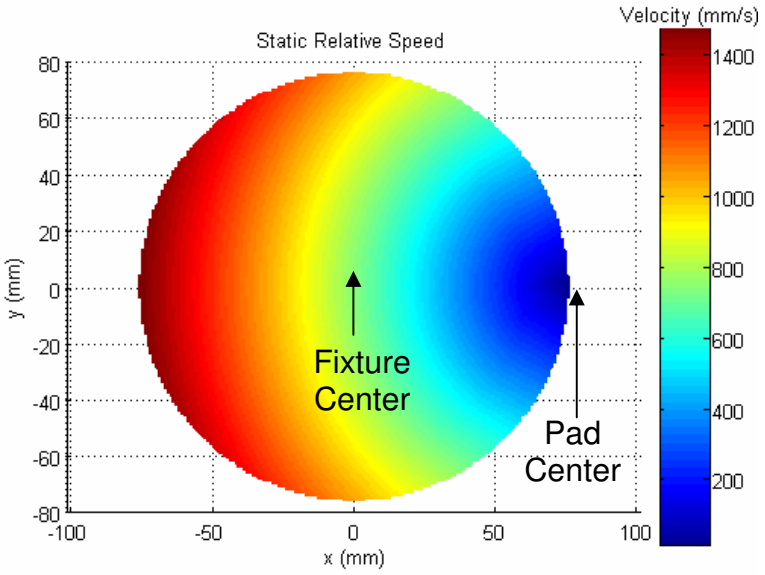

Figure 39. Static Relative Speed

In the diagram, the fixture's center is at the origin, while the pad's center is on the right side at the point of zero relative velocity. All subsequent plots with similar characteristic to this will be plotted in the same manner for consistency purpose. From this plot we can see that there are constant velocity lines at tangential locations within the fixture, centered at the center of the pad. This is expected since the only

velocity component in this diagram is the velocity of the pad. A velocity map for the current rotating polishing setup was also calculated and plotted in Figure 40.

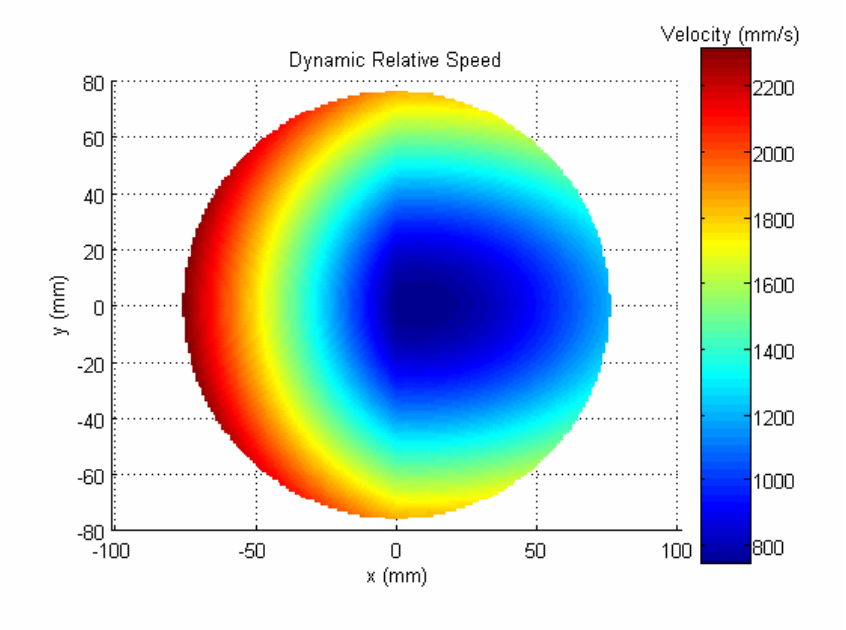

Figure 40. Dynamic Relative Speed

The velocity in a dynamic situation is much more complex than that of a static situation. The lowest velocities are found close to the center, while the highest velocities are still found near the pad's edge and are magnified by the fixture's rotation.

Pressure Measurements

Pressure measurements were taken using the stainless steel fixture in the rotational setup. Static pressure measurements were conducted first and compared to previous results obtained. Afterwards, in-situ rotational experiments were run while varying the experimental variables. Once the general trend for pressure maps was

discovered and tested repeatedly, the stages of the pressure evolution were identified. Then the transition from positive to subambient pressure distributions was more carefully studied. All experiments were run at 150RPM rotational speed for the pad and the fixture and a 100 N load, unless otherwise stated. The results of these experiments are explained below.

Static Measurements

Previous work at the EML laboratory at the Georgia Institute of the Technology had measured fluid pressure at the wafer interface with the wafer fixture not rotating. The results of these experiments showed that strong subambient pressures develop in over 70% of the area under the wafer, with positive pressures occupying the other 30%. These results were obtained with the help of various fixtures containing a variety of sensors. For validation purposes, static pressure experiments were obtained using the pressure fixture developed for this thesis. The data was transmitted wirelessly, as if the fixture were rotating. The fixture was rotated manually at intervals of 60 degree angles to obtain a high enough number of data plots to compose a pressure map. A preexisting fixture, which is directly wired to the computer, was also tested in a similar fashion. This fixture has 20 pressure sensors aligned along the radial and tangential lines of the fixture. Only the plain conditioned pad was tested, since it is known from previous experiments that its profile generates suction pressures. Figure 41 displays the number of points measured during the experiments with all 6 manual rotations to achieve a full map. It also displays the relative position of the fixture to the pad.

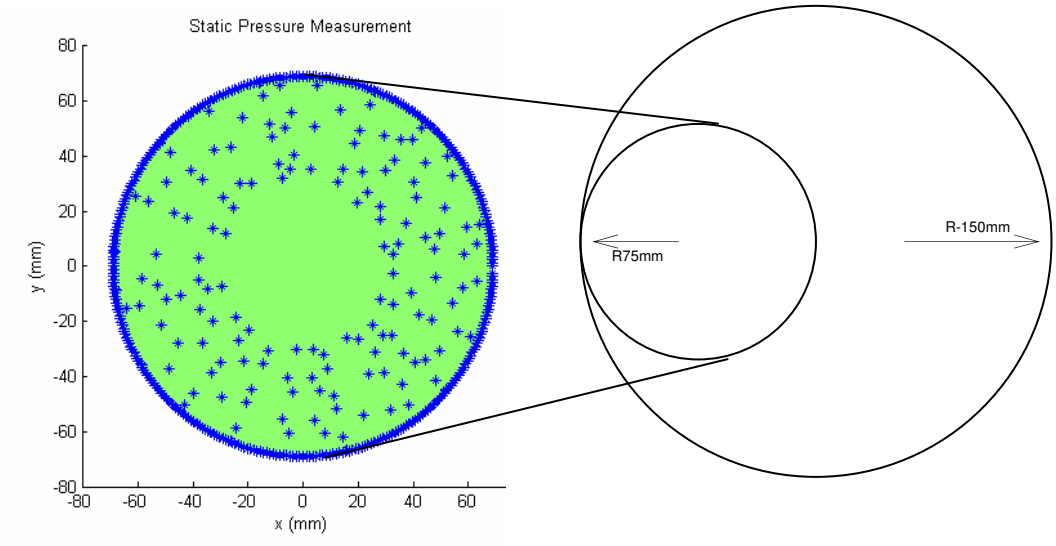

Figure 41. Static Pressure Measurements

Results from the wireless fixture can be seen in Figure 42 (b) and results from the preexisting fixture can be seen in Figure 42 (a). Measurements from both fixtures are consistent with results found by Dr. Ng and published in his dissertation [54]. It is also important to notice that the stress distribution of both are similar, which validates measurements taken by the new fixture. The small differences in the readings could be due to distinct sensor locations between the fixtures, the amount of sensors in each (20 vs. 15 respectively), or small geometric differences between them.

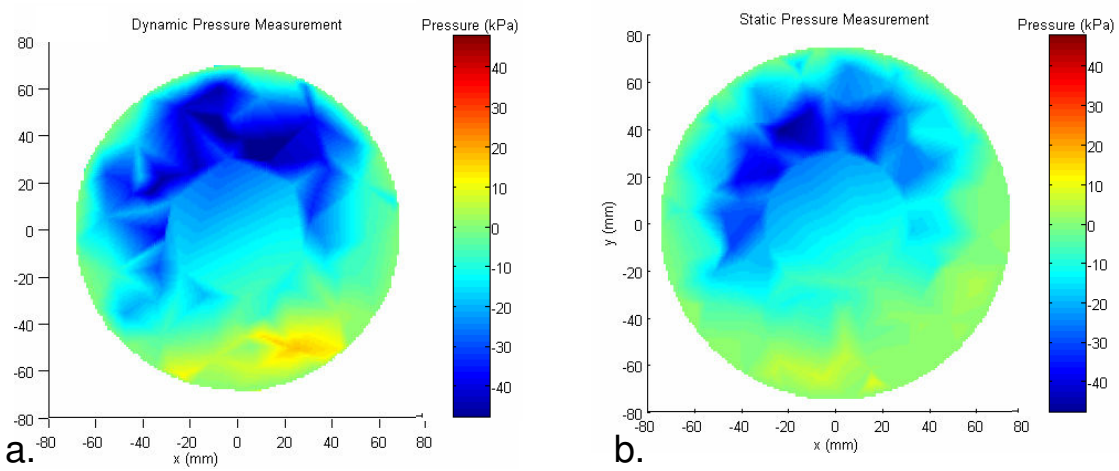

Figure 42. Static Pressure Results with (a) Preexisting and (b) New Fixtures

In-situ Rotational Pressure Results

After verifying that the rotational fixture could transmit data in a static environment, rotational tests were conducted. The only difference in the setup configuration between the rotational and static tests is the rotation of the polishing arm, everything else was kept the same. Rotational experiments were conducted using a full experimental matrix, combining 3 different pad profiles and 3 different slurry flow rates. Results show that the pad's profile influences interfacial fluid pressure, while slurry flow rate has very little effect in the pressure distribution or magnitude. For the plain unconditioned pad, only small positive fluid pressures were detected at the interface. The plain conditioned pad on the other hand displayed strong, center symmetric subambient fluid pressure, which dissipated towards the edges of the fixture. The subambient pressures were mainly concentrated at the center of the fixture. The k-groove pad exhibited no pressure changes, as expected due to its design specifications. The results obtained are very important since they demonstrate the

importance of the pad's surface profile during polishing, as well as show the ability of the k-groove pad to release fluid pressures. It is also worth mentioning that in some cases, the suction pressure between the fixture and the pad was so strong that the polishing head would significantly slow down the conditioned pad's rotational speed. This effect was measured using a photointerrupter with digital signal readout (DT 22400 series). It was calculated that the polishing head still rotates at approximately 150 RPM when this phenomena occurred, while the pad's rotational speed would decrease from 150RPM to about 93 RPM. This was made worse by increasing the normal load on the fixture.

A comparison of typical results obtained with the pressure fixture on all 3 pads is displayed below. Figure 43a represents measurements with the unconditioned pad, the conditioned pad results can be seen in part b, and part c displays results with the k-groove pad. All of the experimental results displayed below were conducted at a 60 ml/min slurry flow rate. The scale on the graphs has been adjusted to facilitate the viewing of the results.

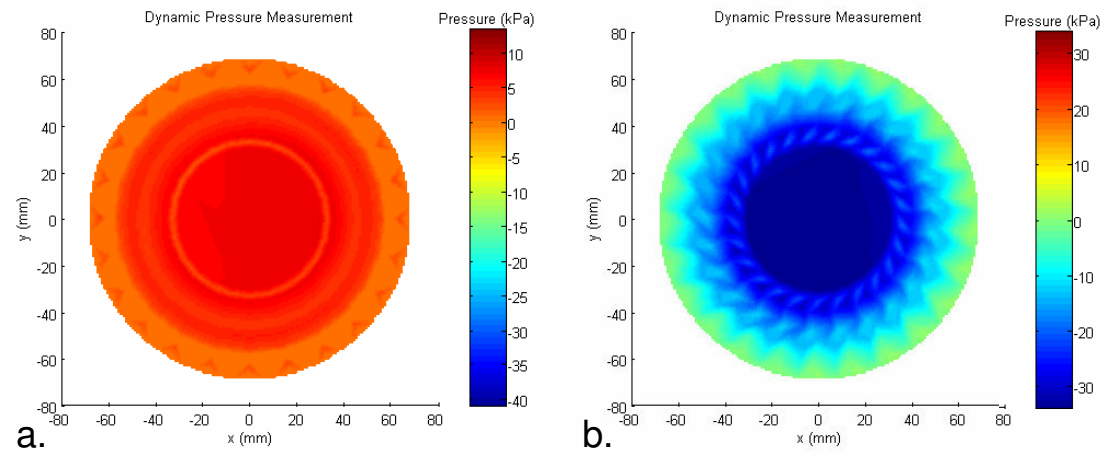

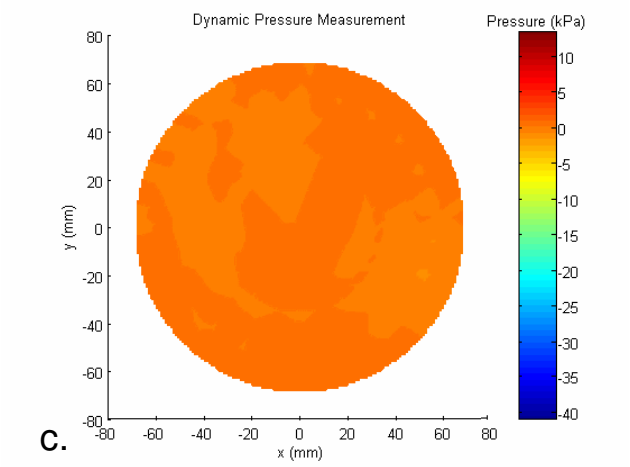

Figure 43. Typical Pressure Results for (a) Unconditioned, (b) Conditioned, and (c) K-groove Pads

As previously stated, the slurry flow rate had no significant impact in the results observed. This is probably due to a lack of slurry starvation at the interface. All the extra slurry which does not fill the voids in the pad and is not transported to the wafer-pad interface is just "squeegeed" out by the fixture's leading edge. Typical results obtained by changing the slurry delivery can be seen in Figure 44, where (a) is 60 ml/min and (b) is 140 ml/min using the conditioned pad. The slurry flow experiments showed little to no change when using the other two pads as well.

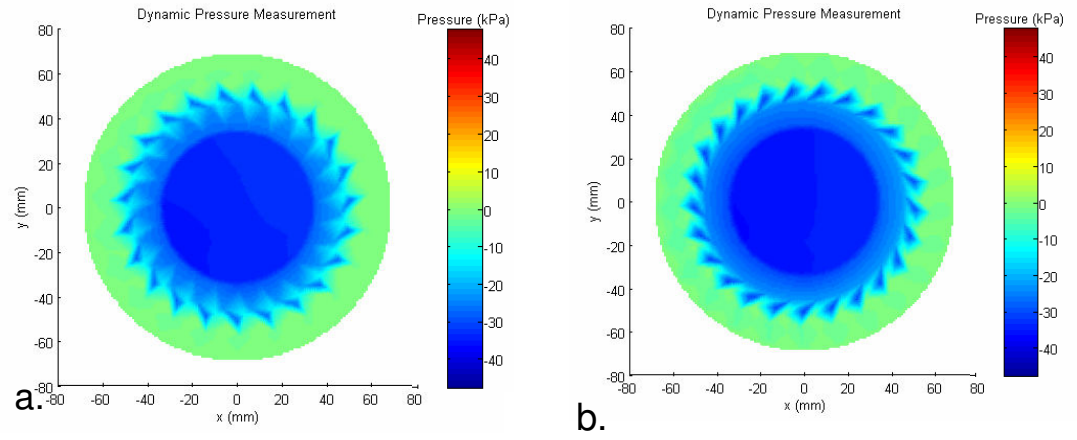

Figure 44. Variations is Pressure with (a) 60 and (b) 140 ml/min Slurry Flow Rates

Stages of Pressure Evolution

The stages in which the pressure develops underneath the fixture is an essential piece of information for the tilt experiments and to understand the process itself. With regards to the tilt experiments, it is important to know if the suction pressures previously observed occur before or after the contact of the pad and fixture under no rotation. This is because if suction pressures develop before any rotation takes place, the tilt measured would not be due to suction pressures, but other factors. To determine the stages of pressure evolution for the conditioned pad, pressure experiments were run while modifying the contact mode between the pad and fixture. The first experiment ran consisted of: First trigger the fixture's photointerrupter 4 times (zeroing data) and bring the fixture down under 100 N normal load, then interrupt 2 more times and start rotating the pad at 150 RPM, interrupt 2 more times and start rotating the fixture. A second experiment was run in a similar fashion except the arm was rotated first, then the polishing pad. The results for the first and second experiments are displayed in Figure 45 (a) and (b) respectively. As previously stated in chapter 4, it is important to know that in these graphs subambient pressures cause a rise in signal while positive pressures cause a decrease in the signal.

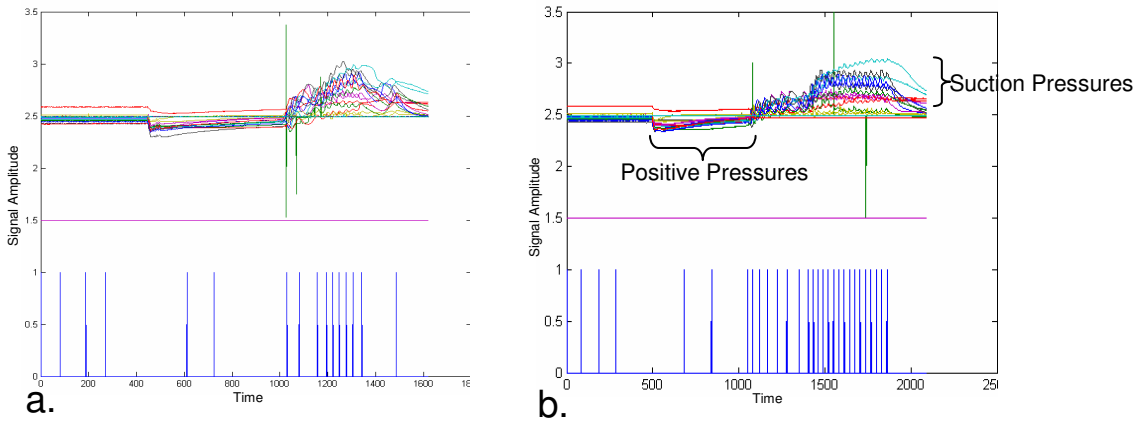

Figure 45. Stage Pressure Evolution

From these graphs it can be seen that in both experiments when the fixture comes in contact with the wet pad under a 100 N normal load, a small positive pressure develops at the interface. It can also be seen that, in both experiments, as one component rotates individually, a sudden drop in pressure occurs, in most cases resulting in subambient pressures. As both components (pad and fixture) start rotating simultaneously, the magnitude of the subambient pressures increases dramatically. These experiments conclude that the subambient pressures are caused by the relative motion of the pad and the fixture and in the absence of rotation, the pressure at the interface is positive as expected since the fluid film partially supports the normal load applied. These results also show that the tilt observed by the capacitive bridge system could be caused by the interfacial fluid pressures.

Transition from Positive to Subambient Pressures

There is a transition from positive to subambient interfacial fluid pressure when the conditioned pad is used. This can be observed in both graphs of Figure 45, as well as in any graph displaying the typical behavior of the fluid with the

unconditioned pad in place. Figure 46 shows a typical fluid pressure reading from the conditioned pad and a rise in pressure when the fixture and the pad first come in contact (initial dip in the data), and a very rapid development of subambient pressure thereafter (sudden rise in sensor output). The experimental data in this graph follows the experimental procedure previously explained in which the interrupter is manually triggered 4 times, then the fixture does about 3 rotations in the air before coming in contact with the pad. By the 7th revolution we can see the positive pressures, which start turning into subambient pressures by around the 10th revolution. Each revolution takes 0.4 seconds. We can also see that the subambient interfacial fluid pressure reaches a steady state in less than 5 seconds. This is consistent throughout the experiments.

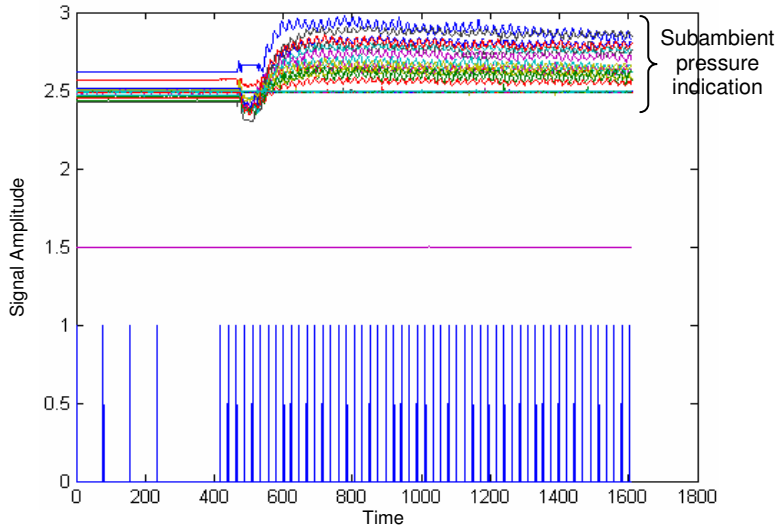

Figure 46. Typical Pressure Measurement of the Conditioned Pad

A better visualization of the pressure evolution results is displayed in Figure 47. The data plots displayed are during: (a) prior to fixture-pad contact, (b)

immediately after fixture-pad contact, (c) 0.4 seconds of contact, (d) 0.8 seconds of contact, and (e) 1.2 seconds of contact. All results were plotted using the same scale for ease of comparison and analysis of the pressure evolution. These plots show that the subambient pressure evolves from the center of the fixture towards the outside, and that in less than 2 seconds of contact this subambient pressure can reach 27.5 kPa.

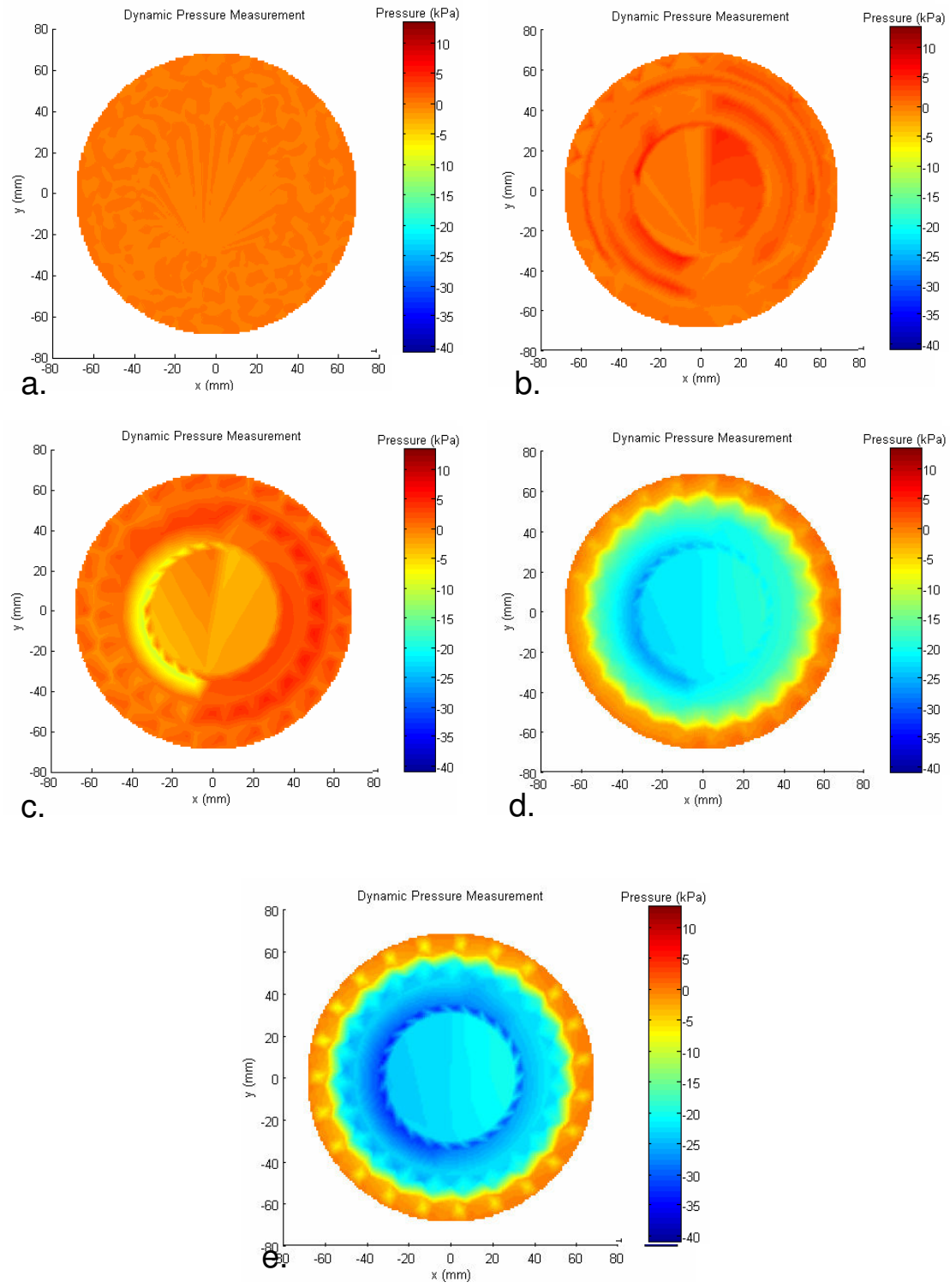

Figure 47. Pressure Evolution Maps

Temperature Measurements

Temperature measurements were taken using the RP fixture in the rotational setup. Several experimental parameters were studied while conducting temperature experiments, including pad topography, slurry flow rate, and slurry type. Temperature changes at the interface were found to be consistent with previous experiments performed [35]. All experiments in this section were conducted at 150 RPM rotational speed of the pad and the polishing head, with a 100 N normal load applied on the fixture. Temperature results are also consistent with the pressure results previously presented.

Slurry Type and Flow Differences

Variations of experimental parameters suggested that slurry delivery has an effect in the temperature development. First, the experiments were run using water to match the previously presented pressure measurements. Temperature was measured at the interface using the fixture, as well as at the trailing edge using an infrared thermometer. Results from the flow rate experiments show similar patterns of temperature change at the interface, with a difference in magnitude. This was true for both slurries. 60 ml/min flow rate generated the most heat, followed by 100 and 140 ml/min respectively. This is due to the cooling that the slurry produces on the pad and at the interface. New incoming slurry is cooler than the pad, the fixture, and old slurry. As the slurry flow increases, the pad and fixture are cooled faster, decreasing the change in temperature at the interface. Figure 48 displays results of 60 vs. 140 ml/min flow rates while using the conditioned pad. Part (a) shows 60 ml/min while part (b) shows 140 ml/min.

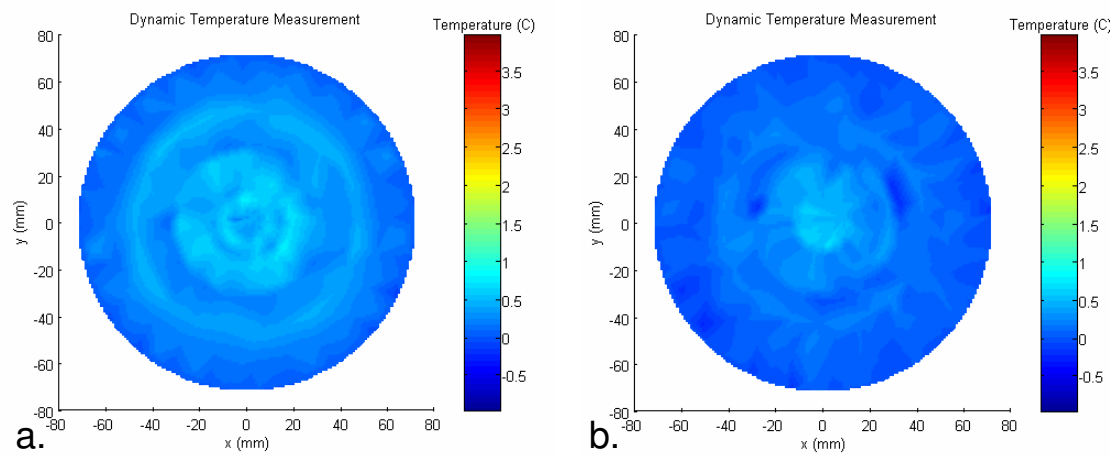

Figure 48. Difference in Temperature at (a) 60 and (b) 140 ml/min Slurry Flow Rate

From these temperature plots, we can see that the temperature of the center of the wafer is higher than the edges by about 1 °C. At first glance, these results looked similar to the pressure experiments and therefore commercial slurry was used to generate higher temperatures. Commercial slurries contain nanoabrasive particles that are used for material removal, which in this case could increase the local temperatures at the wafer interface. As predicted, slurry increased the magnitude of the temperature, but not the distribution. Again, a higher slurry flow rate created a cooling effect which in turn decreased the temperature change at the interface. The most important accomplishment with the slurry is being able to see more clearly if the temperature plots resemble the pressure plots. Results in Figure 49 compare temperature experiments under the same conditions except for the type of slurry. Figure 49a show the results obtained using water, while Figure 49b shows results obtained using slurry. The increase in temperature at the interface can be attributed to the interaction of the

slurry abrasives with the surface of the wafer, presumably under suction pressures. This assumption will be corroborated in the next section.

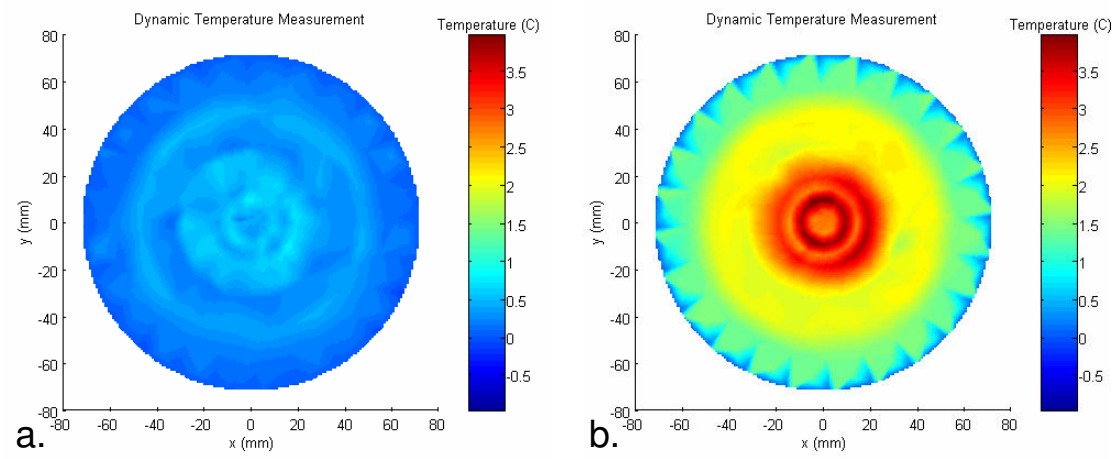

Figure 49. Difference in Temperature using (a) Water and (b) Slurry

Pad Topography Influence in Temperature

Pad topography has a big influence in temperature generation at the wafer-pad interface. Since the influences of slurry type and flow rate have previously been described, only the commercial slurry and 60 ml/sec results will be presented in this section to describe the influence of pad topography. All other results were consistent with the trends previously encountered. This selected condition generates the most amount of heat. Figure 50 displays results of polishing experiments for the (a) unconditioned, (b) conditioned, and (c) k-groove pads. These results show that there is no temperature rise when utilizing the unconditioned pad and very little variation within the k-groove pad. On the other hand, there is a significant temperature variation when polishing with the conditioned pad.

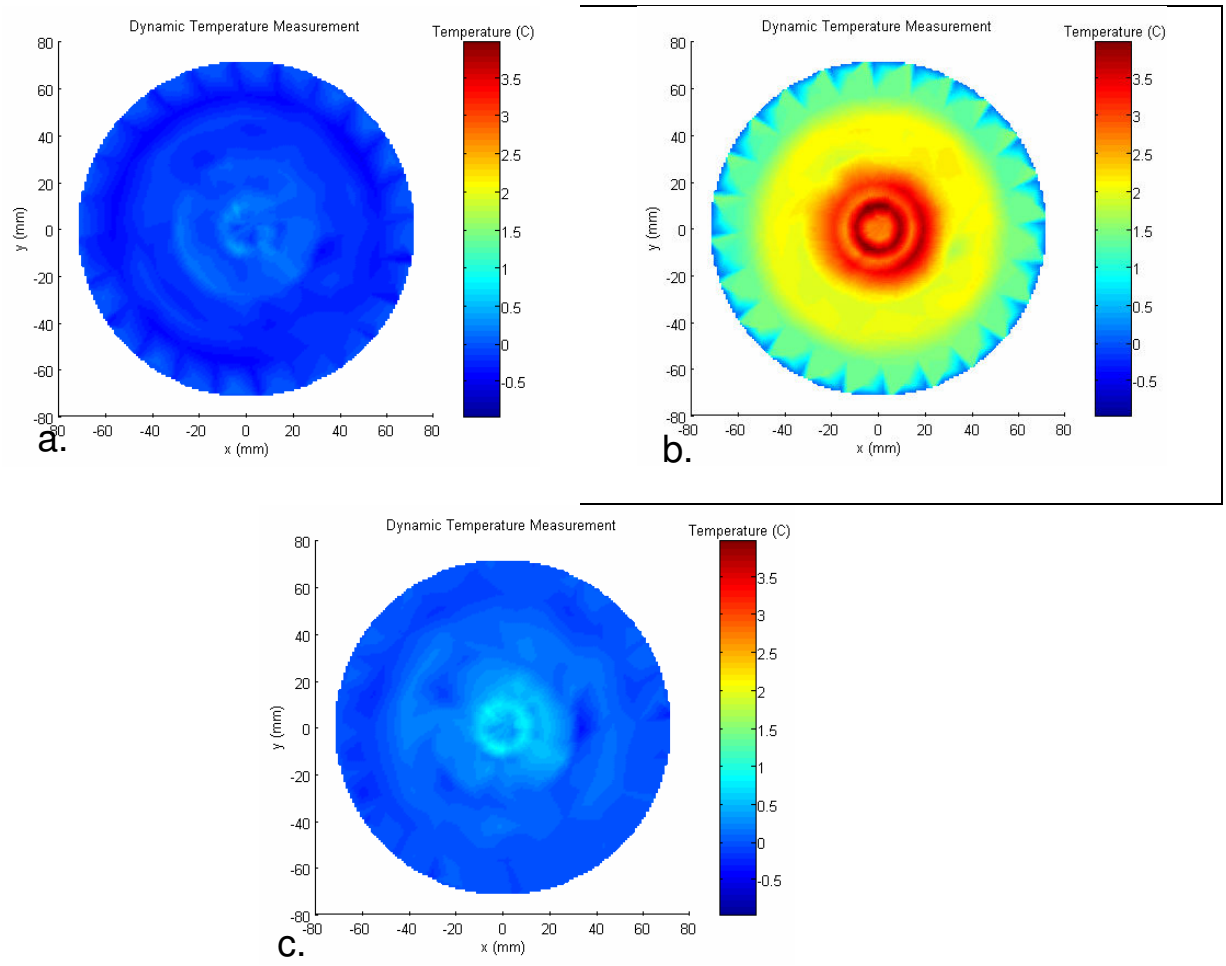

Figure 50. Difference in Temperature using (a) Unconditioned, (b) Conditioned and (c) K-groove Pads

When we compare these results with those found in Figure 43 on page 86, we can see a clear relationship between the heat generation and the fluid pressure at the interface. For (a) the unconditioned pad, small positive pressures resulted in virtually no heat generation (possible hydrodynamic lubrication regime). Figures (b) show that the strong subambient pressures measured at the interface also cause a rise in temperature, particularly at the center of the wafer. We can also observe that at the edges, where the subambient pressure is relieved, the heat generation is much less than at the center. This could be explained by the strong suction pressure bringing the

two surfaces into more intimate contact, which gives an opportunity for the slurry entrenched in the pad to effectively abrade the materials and generate heat in the process. Also the asperity contacts on the pad would be pressed against the wafer, generating more heat. Part (c) shows no pressure developments due to the pad's grooves, which in turn produces very little heat generated. The maximum temperature generated was around 4 °C at the wafer's center. The magnitude of heat generation is consistent with results found by Soorishian *et al* [27][29]. These results are also consistent with polishing results in industry which exhibit center high polishing with a drastic change towards the edge.

Temperature Development at the Interface

Once the various experimental parameters had been tested and their influence in heat generation was established, the development of this temperature was examined. Unlike interfacial fluid pressure, temperature takes some time to develop at the interface. This delay could be due to transition time from positive to negative pressures, pad softening time, or slurry cooling of the interface. Pressure reaches steady state in less than 5 seconds, while temperature takes over 30 seconds to stabilize. Figure 51 displays a graph of the rise in temperatures at the interface. The graph presents approximately 35 seconds of data, at which the temperature has almost completely stabilized throughout the surface of the wafer. This is consistent with results found by Soorishian [29] and Kim [6].

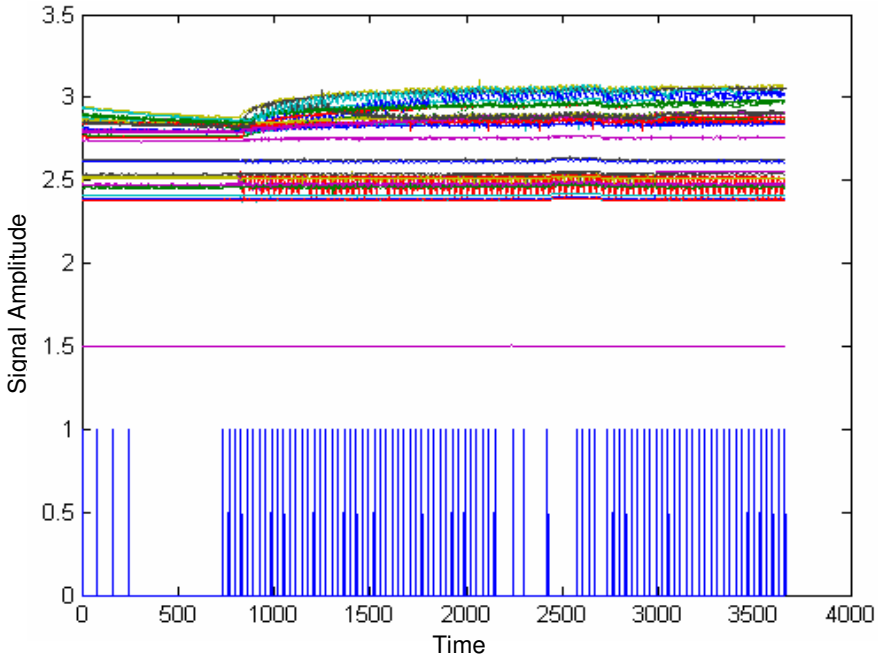

Figure 51. Development of Interfacial Temperature

Tilt Measurements

Tilt measurements were conducted using the capacitive bridge setup and the pressure fixture as a target. Only water was used during tilt experiments to avoid damaging the stainless steel fixture with the abrasive oxidizing slurry. Although water flow rate was not found to have any significant effects on tilt, pad topography was found to have a deep impact in tilt positioning and displacement. Tilt experiments show a clear difference between the pads, especially for the conditioned pad. Several tilt experiments were performed for each pad and the results were very consistent, therefore an average of 3 samples was taken for the 3 pads. Results can be found in Table 4.

Table 4. Tilt Measurement Results

Pad Type	Theta (rads)	Phi (rads)	dz (m)
Unconditioned	5.203	-9.3E-05	3.32E-07
Conditioned	2.394	-3.9E-04	2.35E-05
K-Groove	1.226	7.35E-06	-9.01E-07

As can be observed from the results, the displacement of the center of the fixture is two orders of magnitude greater for the conditioned pad than for the other two topographies. This displacement is over 20 microns in the negative direction, indicating suction. The results for the unconditioned pad show less than 1 µm positive displacement, which can be explained by the small positive pressures measured previously. For the K-groove pad, the displacement was close to 1µm in the negative direction, indicating very little suction present. With respect to angles, results for the conditioned pad were similar to results found by Ng [54] under similar pad topography. The suction of the conditioned pad tends to tilt the fixture towards the leading edge (137 degrees from the x axis) and at an angle of -0.022 degrees with respect to the z axis. For the other two pads, the tilt angle is very small and the position of tilt varies. This variation could be due to the small displacements shown by each sensor, which displays no significant tilt. Table 5 shows a comparison between the results obtained by Ng (in static tilt experiments) and the results obtained with the rotating fixture under similar polishing conditions.

Table 5. Comparison of Dynamic vs. Static Tilt Experiments

Pad Type	Theta (rads)	Phi (rads)	dz (m)
Rotational Tilt	2.394	-3.9E-04	2.35E-05
Static Tilt	0.9338	4.70E-04	2.17E-05

Result Comparison

As previously presented, previous static results for the conditioned pad are similar to the ones measured using the current wireless setup. These results and accompanying mechanical model differ from the results obtained in a rotating environment. This section analyzes and suggests explanations for those differences.

Static Data and Model

Figure 42 displays results obtained during static measurements while using (a) the preexisting fixture and (b) the new pressure sensing fixture with a wireless setup. The results are very similar, suggesting consistency in the readings of the sensors since both systems are very different. In this figure we can see that most of the area under the wafer is covered by subambient fluid pressures and that there is small trace of positive pressures at the trailing edge of the wafer. These results are consistent with the model derived by Ng [54]. This model incorporates surface roughness, contact stresses due to pad deformation, shear flow factors, and other parameters to determine the interfacial fluid pressure. A more in-depth description of the model can be found in the literature review section of this thesis. Figure 52 shows a comparison of experimental results (a) and the results from the model (b). As it can be seen, experimental results are in accordance with theoretical results in magnitude and location. The experimental results diagram is choppy due to sensor relative location when compared to continuous mesh generated by the model for the theoretical results.

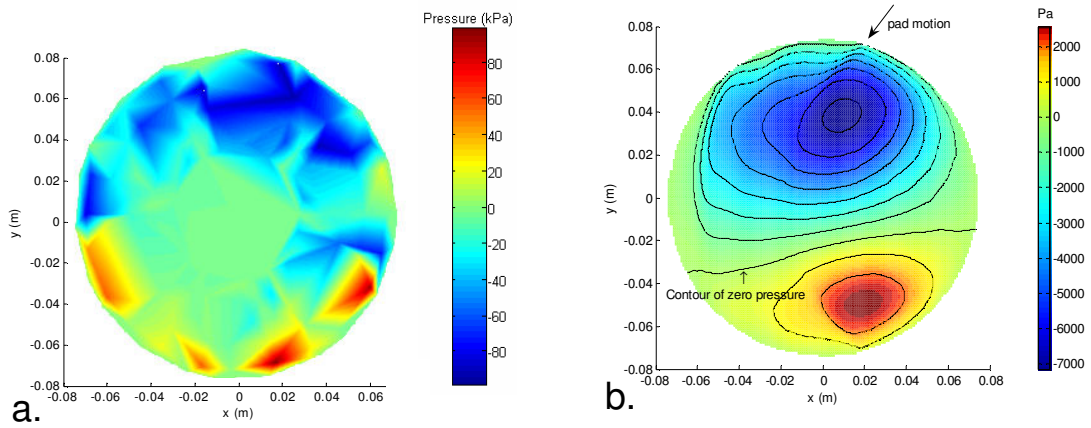

Figure 52. (a) Experimental and (b) Theoretical Static Pressure Results

Rotational Data and Model

As it can be seen in Figure 53, static and rotating interfacial fluid pressure data is not the same. Both diagrams display data obtained using the same fixture, under the same experimental parameters. The difference is that in (a) the fixture is held in place within experiments and rotated manually between experiments to obtain a pressure map of the interface. In (b) the fixture is rotated at 150 RPM using the RotoForce-3 polishing arm of the polishing machine. For static measurements, subambient fluid pressures cover about 70% of the interface while small positive pressures cover the remaining 30% of the area. Subambient pressures are located towards the leading edge and positive pressures towards the trailing edge of the fixture. For dynamic measurements, interfacial fluid pressure appears to be mostly subambient concentrated towards the center, arranged in a close to center symmetric fashion. Results obtained by the rotating fluid pressure fixture are consistent with results obtained with other pressures fixtures connected to the wireless setup for

checking purposes, as well as with temperature results obtained from the RP fixture (previously presented).

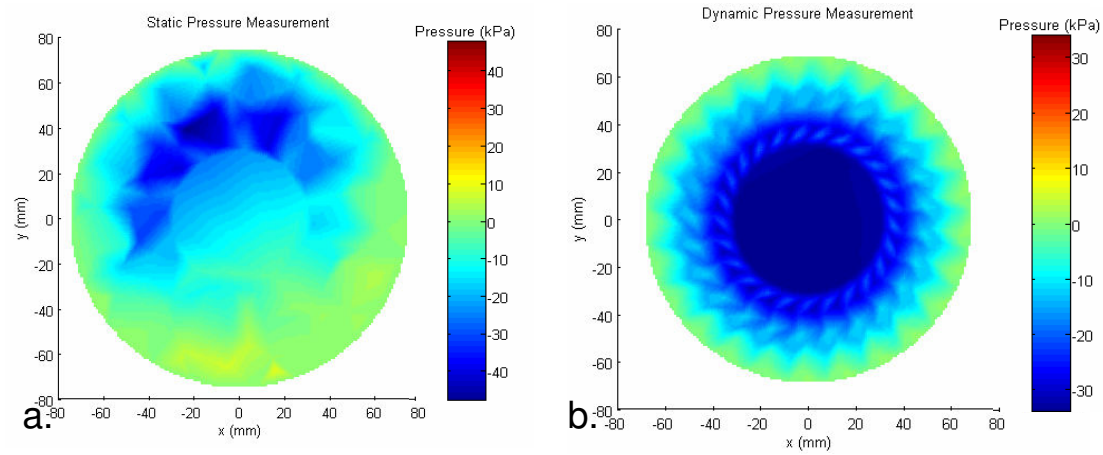

Figure 53. (a) Static and (b) Dynamic Pressure Results

The center symmetric data obtained in a rotating environment can be explained by the period of time it takes for the subambient pressure to dissipate once it is created at the interface. It has been noted through experimentation that suction pressure created at the interface takes several minutes to recede. By rotating the fixture by a fractional amount when the pressure has developed will cause additional subambient pressure to develop in the new region, while the old region still has the previously developed subambient pressure which has not dissipated. As the fixture keeps rotating, the pressure at the interface appears symmetric. This is also in accordance with the model, which uses a steady state form of Reynolds equation to solve for fluid pressure and is not able to capture the time dependence of the pressure creation-dissipation mechanism at the interface.

Material Removal Rate

Material removal rate throughout the wafer surface is a very important parameter in the CMP process, especially in industrial applications. The rate at which material is eroded at the interface determines the amount of time the CMP process is ran, as well as affects line features in patterned wafers. As previously described in Equation 1, Preston's material removal rate model is often used in the semiconductor industry. Preston's equation states that there is a linear relation between material removal and speed and pressure at the interface of the wafer, with an adjustment factor (Preston's coefficient) which covers many other process related parameters. Figure 54 shows material removal maps derived from the use of Preston's equation on each of the pad results. The pressure used was that which was exerted by the normal load applied on the wafers and the pressure exerted by the fluid onto the wafer's surface. The velocity profiles were obtained from calculations as indicated in Equation 10. Preston's coefficient was left at the value of 1, making the values on the scale arbitrary, but comparable with each other.

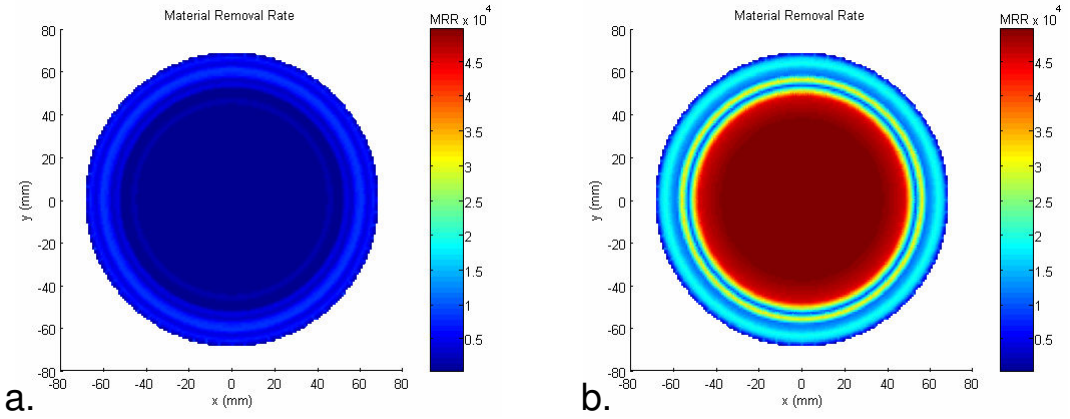

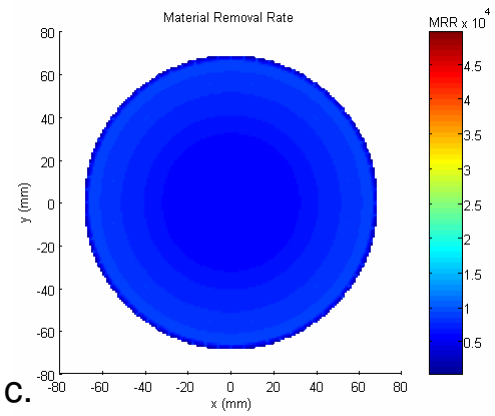

C.

Figure 54. Material Removal Rate for (a)Unconditioned, (b) Conditioned, and (c) K-groove Pads

In the diagrams it can be seen that the conditioned pad which created the most suction pressure has the highest material removal rate. This is due to the strong fluid pressure which increases contact between the pad, the fluid, and the wafer. This profile also has the largest non-uniformity, with high material removal rate towards the center and low material removal rate towards the outside. A polishing process using this pad would have a center high polishing finish, which would be detrimental to the functionality of part of the wafer. The k-groove pad seems to have the most stable process, with very little non-uniformity in the material removal rate profile. It is important to note that there is symmetry in the material removal rate results, despite there being an asymmetric velocity distribution while in rotation. This is due to the units used in the calculations, where pressure effects are much more evident than velocity effects. This kind of material removal rate mappings can be very useful in predicting process completion time and surface defects caused by the CMP process, as well as a control for pad conditioning and profiling in industrial applications.

CHAPTER 7
CONCLUSIONS

A rotating setup for acquiring CMP interfacial fluid pressure and temperature data was developed. The system was designed, assembled, and utilized to characterize the CMP process under several experimental parameters. The system was used to validate previous results obtained by others, as well as to bring new light regarding how temperatures and pressures develop in a rotational setting. The major contributions of this project are:

- Identified that rotational and static interfacial fluid pressures vary in location under the wafer area, but not much in magnitude. In both cases the maximum fluid pressure reached about 42 kPa subambient pressure.
- Water flow rate was not found to be a significant factor in the development of interfacial pressures and only acted as a cooling fluid during temperature tests. This is explained by an absence of water starvation at the interface, in which case the extra water is not entrained between the pad and the wafer and does not aid the material removal process or pressure development.
- Pad topography was demonstrated to have the most significant effects on pressure and temperature variations. This confirms prior work done by Ng [54]. Unconditioned plain pads and k-groove pads were found to have the least amount of pressure and temperature deviations, while the conditioned plain pad had a significant rise in temperature and exhibited subambient pressures at the interface.

- Static pressure data was found to be non-symmetric, with the leading edge having subambient pressures which cover about 70% of the wafer's area. Small positive pressures were found at the trailing edge, occupying about 30% of the area under the wafer. Rotational data shows mostly subambient pressures concentrated at the center and dissipating towards the outside. It was also proven that these pressures develop due to the relative motion of the two interfaces and not during static contact.
- Dynamic temperature measurements show a correlation with the pressure variations. When no pressure develops at the interface, little to no heat is generated. When subambient pressures create suction between the pad and the fixture, there is a rapid buildup of temperatures distributed along the same direction as the subambient pressures. This is explained by the fact that suction pressures bring the pad and the wafer into more intimate contact with each other, allowing the pad asperities and the slurry abrasive particles to more effectively polish the material and generate heat. The maximum amount of heat generation was about 4 °C at the wafer's center.
- Subambient pressures develop within 5 seconds of contact of the pad-wafer interface while in relative motion and stabilize soon after. Temperature at the interface gradually develops and only reaches steady state after 30 seconds into the process. This could be due to the continued cooling effect of the new incoming slurry and the dependency of temperature upon interfacial pressure.

- K-groove pads show the lowest non-uniformity in material removal rate, while the strong suction pressures produced by the plain conditioned pad accelerate material removal rate and increase within wafer non-uniformity.
- Tilt experiments show that the suction of the conditioned pad brings the fixture down approximately 20 μm. This does not occur with the other pads, suggesting little to no pressure buildup at the interface.

REFERENCES

[1] Wang, Y.L., C. Liu, M.S. Feng, W.T. Tseng, "The Exothermic Reaction and Temperature Measurement for Tungsten CMP Technology and its Applications on Endpoint Detection" *Materials Chemistry and Physics*, Vol. 52, 1998.

[2] Nanz, Gerd., L.E. Camilletti. "Modeling of Chemical-Mechanical Polishing: A Review" *IEEE Transactions on Semiconductor Manufacturing,* Vol. 8, November 1999. p382-389

[3] Ng, Sum Huan., R. Hight, C. Zhou, I. Yoon, S. Danyluk. "Pad Soaking Effect on Interfacial Fluid Pressure Measurements during CMP" *ASME Journal of Tribology,* Vol. 125, July 2003. p582-586

[4] Levert, J.A, S. Danyluk, J. Tichy, "Mechanism for Subambient Interfacial Pressures While Polishing With Liquids" *ASME Journal of Tribology*, Vol. 122, 2000. p450-457

[5] Coppeta, J., C. Rogers, L. Raez, A. Philipossian, F.B Kaufman, "Investigating Slurry Transport Beneath a Wafer during Chemical Mechanical Polishing Process" *Journal of The Electrochemical Society*, Vol. 147, 2000. p1903-1909

[6] Kim, H.J., H.Y. Kim, H.D. Jeong, E.S. Lee, Y.J. Shin, "Friction and Thermal Phenomena in Chemical Mechanical Polishing" *Journal of Materials Processing Technology,* Vol.130-131, 2002. p334-338

[7] Parikh, P.J., "Chemical Mechanical Planarization: An Analysis of Variables" *Chemical Mechanical Planarization I,* Vol 96-22, 1997. p79-90

[8] Koizumi, S., K. Kato, "New Method to Evaluate Stacked Polishing Pad for CMP" *KTECH Research Cop,* 2000.

[9] Lu, H., Y. Obeng, K.A. Richardson, "Applicability of Dynamic Mechanical Analysis for CMP Polyurethane Pad Studies" *Materials Characterization*, Vol. 49, 2003. p177-186

[10] Li, Weidan., D.W. Shin, M. Tomozawa, S.P. Murarka, "The Effect of the Polishing Pad Treatments on the Chemical-Mechanical Polishing of SiO_2 Films" *Thin Solid Films,* 270, 1995. p601-606

[11] Castillo-Mejia, D., J. Kelchner, S. Beaudoin, "Polishing Pad Surface Morphology and Chemical Mechanical Planarization" *Journal of the Electrochemical Society,* Vol. 151, 2004. G271-G278

[12] Borucki, L., "Mathematical Modeling of Polish-Rate Decay in Chemical-Mechanical Polishing" *Journal of Engineering Mathematics,* Vol. 43, 2002. p105-114

[13] Castillo-Mejia, D., S. Gold, V. Burrows, S. Beaudoin, "The Effect of Interactions between Water and Polishing Pads on Chemical Mechanical Polishing Removal Rates" *Journal of the Electrochemical Society, Vol 150, 2003, G76-82*

[14] Castillo-Mejia, D., S. Gold, V. Burrows, S. Beaudoin, "Interactions between Water and Polishing Pads" *Chemical Mechanical Planarization V, Vol 2002-1, 2002. p26-29*

[15] Obeng, Y.S., J. Ramsdell, S. Machinsky, H. Lu, I. Li, K.M. Forsthoefel, K. Richardson, S. Seal, "Characterization of 'In-Process' Degradation of Polyurethane CMP Pads" *Chemical Mechanical Planarization V*, Vol 2002-1, 2002. p13-25

[16] Achuthan, K., J. Curry, M. Lacy, D. Campbell, S.V Babu, "Investigation of Pad Deformation and Conditioning during the CMP of Silicon Dioxide Films" *Journal of Electronic Materials,* Vol. 25 1996. p1628-1632

[17] Evans, D.R., M.R. Oliver, "Rotational Averaging of Material Removal During CMP" *Chemical Mechanical Polishing 2001-Advances and Future Challenges*, Vol 671, 2001. M1.4.1-M1.4.7

[18] Ramsdell, J., S. Seal, I. Li, K.A. Richardson, V. Desai, W.G. Easter "Surface Characterization of Polyurethane Pads used in Chemical Mechanical Polishing (CMP)" *Chemical Mechanical Planarization V, Vol 2002-01, 2001.* p102-113

[19] Oliver, M.R., R.E. Schmidt, M. Robinson, "CMP Pad Surface Roughness and CMP Removal Rate" *Chemical Mechanical Planarization IV*, Vol 2000-26, 2001. p77-83

[20] Hooper, B.J., G. Byrne, S. Galligan, "Pad Conditioning in Chemical Mechanical Polishing" *Journal of Materials Processing Technology,* No. 123, 2002. p107-113

[21] Machinski, S., K. Richardson, W. Easter, "Microstructural Characterization of CMP Polyurethane Polishing Pads" *Chemical Mechanical Planarization IV*, Vol 2000-26, 2001. p84-93

[22] Iqbal, A., R.R. Sudipto, "Pad Conditioning in Interlayer Dielectric CMP" *Solid State Technology,* Vol. 40, 1997. p1-4

[23] Dyer, T., J. Schlueter, "Characterizing CMP Pad Conditioning using Diamond Abrasives" *Micro*, Vol. 20, 2002. p47-54

[24] Lawing, S.A., "Polish Rate, Pad Surface Morphology and Pad Conditioning in Oxide Chemical Mechanical Polishing" *Rodel, Inc.*

[25] Clark, A.J., K.B. Witt, R.L. Rhoades, "Oxide Removal Rate Interactions between Slurry, Pad, Downforce, and Conditioning" *Rodel, Inc.*

[26] Tsai, T. C., P.H. Lo, F.L Jaung, C. Chung, C.Y. Lee, E. Hsu, C.L Hsu, L. M. Liu, "The Effect of Pad Temperature on Manufacturing Process Control of W-CMP" *Chemical Mechanical Planarization in IC Device Manufacturing III*, Vol 99-37, 2000. p434-439

[27] Sorooshian, J., D. DeNardis, L. Charns, Z. Li, F. Shadman, D. Boning, D. Hetherington, A. Philipossian, "Arrhenius Characterization of ILD and Copper CMP Processes" *Journal of the Electrochemical Society* Vol. 151, 2004. G85-G88

[28] Borucki, L., Z. Li, A. Philipossian, "Heating and Convection in Copper Polishing" *Chemical Mechanical Planarization VI*, Vol 2003-21, 2003. p61-67

[29] Sorooshian, J., D. Hetherington, A. Philipossian, "Effect of Process Temperature on Coefficient of Friction during CMP" *Electrochemical and Solid-State Letters*, Vol. 7, 2004. G222-G224

[30] Tregub, A., M. Moinpour, J. Sorooshian, "Effect of Temperature on Thermoanalytical Properties of Polishing Pads" *Intel Corporation*

[31] Sikder, A.K., I.M. Irfan, A. Kumar, A. Belyaev, S. Ostapenko, M. Calves, J.P. Harmon, J.M. Anthony, "Evaluation of Mechanical and Tribological Behavior, and Surface Characteristics of CMP Pads" *Chemical-Mechanical Polishing 2001-Advances and Future Challenges*, Vol. 671, 2001. M1.8.1-M1.8.7

[32] Karaki, T., J. Watanabe, "Effect of Frictional Heat on Removal Rate in Mechanochemical Polishing of Crystals used in Electronics" *ASME Wear of Materials,* 1983. p227-234

[33] Hocheng, H., Y.L. Huang, L.J. Chen, "Kinematic Analysis and Measurement of Temperature Rise on a Pad in Chemical Mechanical Planarization" *Journal of the Electrochemical Society,* Vol. 146, 1999. p4236-4239

[34] Wang, Y.L., C. Liu, M.S. Feng, W.T. Tseng, "The Exothermic Reaction and Temperature Measurement for Tungsten CMP Technology and its Application on Endpoint Detection" *Materials Chemistry and Physics,* Vol. 52, 1998. p17-22

[35] Cornely, J., C. Rogers, V. Manno, A. Philipossian, "Real-Time Measurement of Temperature In the Pad-Wafer Region during CMP" *Chemical Mechanical Planarization V*, Vol. 2002-1, 2002. p184-192

[36] Janzen, J.W., R.J. Hanestad, "Extension of Polish Pad Lifetime Using Wafer Backpressure" *Semiconductor International,* Vol. 19 June 1996. p147-150

[37] Melvin, J.W., N.P. Suh, "Axiomatic Design of a Chemical Mechanical Polishing (CMP) Wafer Carrier with Zoned Pressure Control" *ASME Micro-Electromechanical Systems Division Publication,* 2002. p291-300

[38] Sasaki, Y., H. Aoyama, I. Inasaki, H. Miyairi, H. Shibaya, "Evaluation of Effective CMP Conditions by Estimation of Pressure Distribution on Semiconductor Wafer" *American Society for Precision Engineering,* Vol. 17, 1998. p92-95

[39] Sorooshian, J., L. Borucki, R. Timon, D. Stein, D. Boning, D. Hetherington, A. Philipossian, "Estimating the Effective Pressure on Patterned Wafers during STI CMP" *Electrochemical and Solid-State Letters*, Vol 7, 2004. G204-G206.

[40] Zhang, Y., P. Parikh, P. Golubtsov, B. Stephenson, M. Bonsaver, J. Lee, M. Hoffman, 'Wafer Shape Measurement and its Influence on Chemical Mechanical Planarization" *Chemical Mechanical Planarization I*, Vol 96-22, 1997. p91-96

[41] Bullen, D., A. Scarfo, A. Koch, D.P.Y Bramono, J. Coppeta, L. Racz, "In Situ Technique for Dynamic Fluid Pressure Measurements during Chemical Mechanical Polishing" *Journal of The Electrochemical Society*, Vol 147, 2000. p2741-2743

[42] Zhou, C., L. Shan, J.R. Hight, S. Danyluk, "Influence of Colloidal Abrasive size on Material Removal Rate and Surface Finish in SiO2 Chemical Mechanical Polishing" *Journal of the Society of Tribologists and Lubrication Engineers*, April, 2002. p35-41

[43] Ng, S.H, C.M. Zettner, C. Zhou, I.H. Yoon, S. Danyluk, M. Sacks, M. Yoda, "Nanoparticulate and Interfacial Mechanics in Confined Geometries Typical of Chemical-Mechanical Planarization" *ASME International Mechanical Engineering Congress & Exposition*, November, 2003. p1-8

[44] Shan, L., J.A. Lavert, L. Meade, J. Tichy, S. Danyluk, "Interfacial Fluid Mechanics and Pressure Prediction in Chemical Mechanical Polishing" ASME *Journal of Tribology*, Vol. 122, 2000. p539-543

[45] Levert, J.A., F. Mess, L. Grote, M. Dmytrychenko, L. Cook, S. Danyluk, "Slurry Film Thickness in Float and Semi-Permeable and Permeable Pad Geometries" *Proceedings of the International Tribology Conference*, 1995.

[46] Mess, F., J.A. Levert, S. Danyluk, "Vertical Differential Displacements at a Pad/ Sapphire Interface during Polishing" *Wear of Materials*, 1997. p311-315

[47] Tichy, J., J.A. Lavert, L. Shan, S. Danyluk, "Contact Mechanics and Lubrication Hydrodynamics of Chemical Mechanical Polishing" *Journal of the Electrochemical Society*, Vol 146, 1999. p1523-1528

[48] Shan, L., S. Danyluk, J.A. Lavert, "Interfacial Pressure Measurements at Chemical Mechanical Polishing Interfaces" *Materials Research Society Symposium Proceedings*, Vol 566, 2000. p187-195

[49] Danyluk, S., "Chemical Mechanical Polishing Research" *Final Report to Motorola, Inc.*, July 20, 2000. p1-19

[50] Shan, L., C. Zhou, S. Danyluk, "Mechanical Interactions and their Effect on Chemical Mechanical Polishing" *IEEE Transactions on Semiconductor Manufacturing*, Vol. 14, 2001. p207-213

[51] Higgs, C.F, S.H. Ng, I. Yoon, L. Shan, L. Yap, S. Danyluk, "Mechanical Modeling of the 2D Interfacial Slurry Pressure in CMP" *Materials Research Society Symposium Proceedings*, Vol. 767, 2003. p305-312

[52] Ng, S.H., I. Yoon, C.F. Higgs, S. Danyluk, "Wafer-Bending Measurements in CMP" *Journal of the Electrochemical Society*, Vol. 151, 2004. G819-G823

[53] Levert, J.A., "Interface Mechanics of Chemical Mechanical Polishing for Integrated Circuit Planarization" *PhD Dissertation*, Georgia Institute of Technology, 1997.

[54] Ng, S.H, "Measurements and Modeling of Fluid Pressures in Chemical Mechanical Polishing" *PhD Dissertation*, Georgia Institute of Technology, 2005.

[55] Hight, J.R. "Interfacial Fluid Pressure and Pad Viscoelasticity during Chemical Mechanical Polishing" *Master's Thesis*, Georgia Institute of Technology, 2002.